Available online at www.sciencedirect.com
ScienceDirect
Lithos 96 (2007) 205–224
LITHOS
www.elsevier.com/locate/lithos

Post-collisional adakites in south Tibet: Products of partial melting of subduction-modified lower crust

Zhengfu Guo [a,b,*], Marjorie Wilson [b], Jiaqi Liu [a]

[a] Institute of Geology and Geophysics, Chinese Academy of Sciences, P.O. Box 9825, Beijing 100029, PR China
[b] School of Earth and Environment, University of Leeds, Leeds LS2 9JT, UK

Received 9 December 2005; accepted 5 September 2006
Available online 29 December 2006

Abstract

Post-collisional (26.2 to 10.1 Ma) adakites occur within the Lhasa terrane of the southern Tibetan Plateau in an E–W trending, 1500 km long, magmatic belt. Outcrops are small and restricted within N–S-trending rift zones (grabens); they include both extrusive and intrusive facies. The adakites have high SiO_2 (59–70 wt.%), Al_2O_3 (15–18 wt.%) and Sr (317–1133 ppm) contents and Sr/Y ratios (44–162), and low Y (4.2–12.9 ppm) and HREE (e.g. Yb < 0.9 ppm) concentrations. Their MORB-normalised incompatible element patterns exhibit strong enrichments in large ion lithophile elements (LILE) relative to high field strength elements (HFSE). The combined trace element and Sr–Nd–Pb isotope characteristics of the adakites suggest that their source was mafic-intermediate lower crust formed during a preceding stage (153–40 Ma) of active continental margin magmatism. Lower crustal melting was primarily induced by the conduction of heat from contemporaneous potassic–ultrapotassic magmas produced by partial melting in the asthenosphere or lower lithosphere. Trace element modelling calculations suggest that the adakites are the products of 5–10% partial melting of garnet-bearing amphibolite facies meta-igneous rocks. Differences in the LILE contents and Sr–Nd isotope compositions of adakites sampled to the east and west of 86° E can be attributed to variable degrees of partial melting of the lower crust and mixing between potassic–ultrapotassic magmas and lower crustal melts. Extensional collapse of the Tibetan Plateau may have contributed to partial melting of the lower crust and the formation of the potassic–ultrapotassic magmatism by decompression melting of a thin asthenospheric mantle wedge above a subducted slab of Indian continental margin lithosphere. The oldest age of the post-collisional adakites and contemporaneous potassic–ultrapotassic magmatism in the Lhasa terrane may, therefore, provide constraints on the timing of initiation of tectonic collapse in the southern part of the plateau.

Keywords: Tibetan Plateau; Adakite; Subduction-modified lower crust; Trace element model; Uplift

1. Introduction

Uplift of the Tibetan Plateau, post-dating India–Asia collision, is considered to be one of most important geological events worldwide. Understanding the cause of post-collisional magmatism in the Tibetan Plateau can provide important constraints on both the mechanism of plateau uplift and the nature of the source region of the magmas (Pearce and Mei, 1988; Turner et al., 1993, 1996; Miller et al., 1999; Williams et al., 2001, 2004; Guo et al., 2005, 2006). In addition, such understanding may provide greater insights into the nature of the magmatic plumbing system in a young orogenic belt.

* Corresponding author. Institute of Geology and Geophysics, Chinese Academy of Sciences, P.O. Box 9825, Beijing 100029, PR China. Tel.: +86 10 62007334; fax: +86 10 62032495.
E-mail address: zfguo@mail.iggcas.ac.cn (Z. Guo).

0024-4937/$ - see front matter © 2006 Elsevier B.V. All rights reserved.
doi:10.1016/j.lithos.2006.09.011

Adakites have only recently been recognized in south Tibet, forming part of a suite of post-collisional magmatic rocks (e.g. Chung et al., 2003; Hou et al., 2004). The geochemical and isotopic characteristics of the adakites can provide important constraints on their petrogenesis and geodynamic setting, which is highly controversial. Chung et al. (2003) and Hou et al. (2004) proposed that the adakites originated by partial melting of thickened lower crust, whereas Qu et al. (2004) ascribed their petrogenesis to partial melting of subducted oceanic crust. Hou et al. (2004), however, conceded that they could not entirely rule out the possibility that a subducted slab of Neotethys oceanic crust was the source of the adakites. The lack of detailed field sampling and of petrological and geochemical data has precluded further constraints on the petrogenesis of the south Tibetan adakites. In this study, we report new geochemical data for adakites from the Lhasa terrane of southern Tibet; these data, combined with previous geochemical and geophysical data, allow us to develop a more robust petrogenetic model.

2. Geological setting

The Lhasa terrane in south Tibet, is bounded by the Bangong–Nujiang suture (BNS) to the north and by the Indus-Yalu suture (IYS) to the south (Fig. 1). The Bangong–Nujiang ocean, now represented by the BNS, probably subducted southwards beneath the Lhasa terrane during Late Paleozoic to Early Cretaceous times (e.g. Pan and Ding, 2004; Qiu et al., 2004), although Kapp et al. (2003) proposed that it subducted northwards beneath the Qiangtang terrane in Late Jurassic times. Closure of the Bangong–Nujiang ocean and continental collision between the Qiangtang terrane to the north and the Lhasa terrane to the south, generating the BNS, are thought to have occurred either in the Late Jurassic–Early

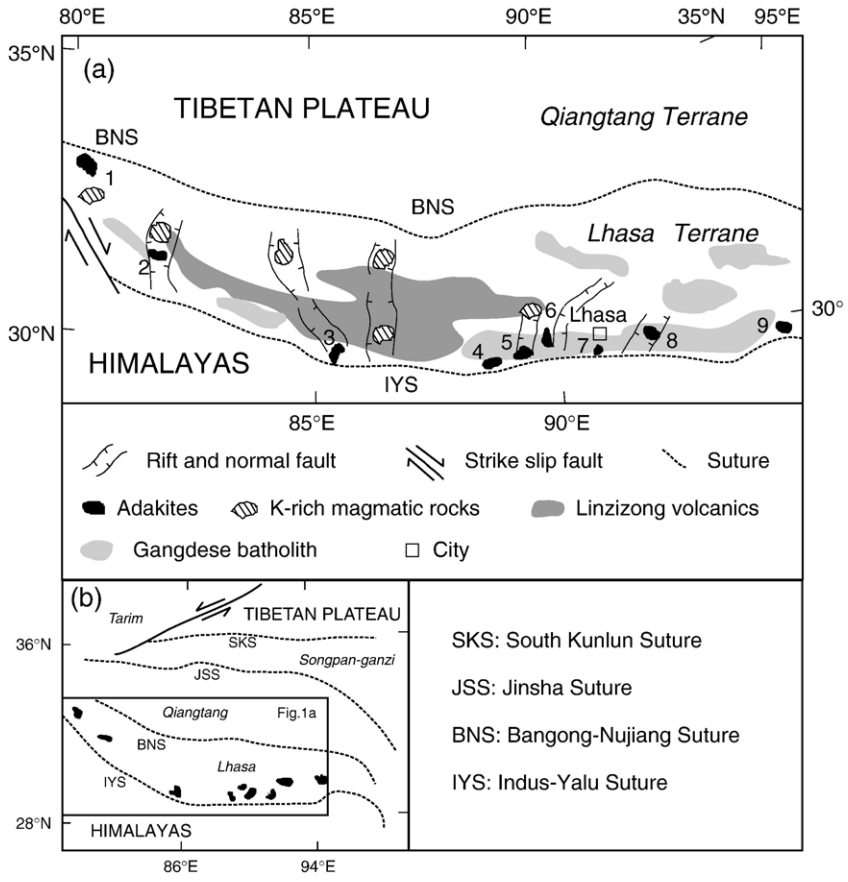

Fig. 1. (a) Map showing the distribution of post-collisional adakites in the southern Tibetan Plateau (modified from Yin and Harrison, 2000; Blisniuk et al., 2001; Chung et al., 2003; Zhang and Ding, 2003; Hou et al., 2004). BNS, Bangong–Nujiang suture; IYS, Indus–Yalu suture. Numbers indicate the names of the volcanic fields (or intrusive bodies). 1: Shiquanhe; 2: Gegar; 3: Daggyai; 4: Xigaze; 5: Wuyu; 6: Majiang; 7: Nanmu; 8: Jiama; 9: Linzhi. (b) Map showing the tectonic outline of the Himalaya-Tibet orogenic belt (modified from Yin and Harrison, 2000; Williams et al., 2004). The rectangle shows the location of (a).

Cretaceous (Kapp et al., 2003) or the Middle Cretaceous (Pan et al., 1997, 2004; Pan and Ding, 2004). Neotethyan ocean crust, indicated by the IYS, has subducted northwards beneath the Lhasa terrane since the Late Jurassic to Early Cretaceous (BGMRTAR, 1993; Aitchison et al., 2000); this subduction resulted in extensive Andean-type calc-alkaline magmatism in the Lhasa terrane (Linzizong volcanics and Gangdese batholith; Fig. 1) which ranges in age from 153 to 40 Ma (Scharer et al., 1984; Coulon et al., 1986; Murphy et al., 1997; Mo et al., 2003). Collision of the Indian and Asian continents started at ~50 Ma in the East-Central Himalaya (Zhu et al., 2005). The Lhasa terrane, the southernmost part of the Asian continent, has been part of the Himalaya–Tibet orogenic belt since the India–Asia collision. Zhou and Murphy (2005) have suggested, on the basis of seismic tomography data, that at the present day there is a thin asthenospheric mantle wedge located above a slab of northward underthrusting Indian continental lithosphere beneath the Tibetan Plateau. They have also proposed that there is a difference in the angle of subduction of the underthrust Indian continental lithosphere to the east and west of ~85° E; subduction is steeper to the east and shallower to the west. In the areas of shallower subduction, the asthenospheric wedge is much thinner and the underthrust Indian lithosphere effectively underplates the Tibetan lithosphere, doubling its thickness.

Post-collisional igneous activity in south Tibet includes both potassium-rich (potassic and ultrapotassic) magmatic rocks and adakites (Fig. 1). Whilst there have been a number of studies on the potassic and ultrapotassic magmatic rocks (e.g. Turner et al., 1996; Miller et al., 1999; Williams et al., 2001, 2004), few data are available in the literature for the southern Tibetan adakites (e.g. Chung et al., 2003; Hou et al., 2004). Adakites are widespread in the Lhasa terrane, forming a ~1500 km long belt, sub-parallel to the IYS. Individual outcrops, with small areal extents (less than 5 km^2 to about 100 km^2), are located within a series of north–south-trending grabens bounded by normal faults (Fig. 1). The adakites range from 26.2 to 10.1 Ma in age, based on $^{40}Ar/^{39}Ar$, K–Ar, Rb–Sr and single-crystal zircon U–Pb dating (Coulon et al., 1986; Yin et al., 1994; Miller et al., 1999; Williams et al., 2001; Chung et al., 2003; Hou et al., 2004; Williams et al., 2004). They are contemporaneous with potassic and ultrapotassic magmatism from 25.4 to 8.2 Ma within the Lhasa terrane (e.g. Miller et al., 1999; Williams et al., 2001; Ding et al., 2003; Nomade et al., 2004; Williams et al., 2004).

Samples were collected from each of the outcrops of adakite indicated in Fig. 1; their petrographic characteristics are summarized in Table 1. In order to determine if there are any geochemical differences related to the geometry of subduction the samples have been divided into two groups (i.e. east or west of 86° E). Zhou and Murphy (2005) consider that the change in the geometry of the subduction system occurs at 85° E; however, since the adakites in the Daggyai area (Fig. 1) are more similar to those further to the west we have used 86° E as the dividing line.

3. Petrography

The Lhasa adakites consist of small volume porphyries, dykes, plugs and lava flows. They have porphyritic textures with phenocrysts of clinopyroxene, amphibole, plagioclase feldspar, alkali feldspar, biotite, quartz, zircon and Fe–Ti oxide; the groundmass includes plagioclase, alkali feldspar, biotite, quartz, zircon, Fe–Ti oxide, titanite, apatite and glass (Table 1).

Table 1
Phenocryst and groundmass mineral assemblages of the Lhasa terrane adakites

Field no.	Sample no.	Locality	Mg-no.	Phenocrysts	Groundmass
1	ZF09	Shiquanhe	0.70	Bi+Pl+Am+Cpx	Bi+Pl+Sani+Ap+Fe–Ti+G
2	GUO62	Gegar	0.63	Bi+Pl+Am+Sani	Bi+Sani+Ap+Fe–Ti+G
2	GUO51	Gegar	0.65	Pl+Am+Sani	Bi+Sani+Ap+Fe–Ti
3	GUO48	Daggyai	0.64	Am+Bi+Pl+Qz+Fe–Ti	Sani+Am+Qz+G
4	GUO37	Xigaze	0.55	Pl+Sani+Am	Sani+Pl+Qz+Fe–Ti+G
5	G09	Wuyu	0.60	Bi+Sani+Pl+Qz	Bi+Sani+Qz+Ap+Fe–Ti
6	ZFG17	Majiang	0.73	Am+Bi+Pl+Sani+Qz+Zr+Fe–Ti	Bi+Sani+Qz+Fe–Ti+Tit+Zr
7	G006	Nanmu	0.63	Pl+Sani+Bi+Qz+Fe–Ti	Pl+Sani+Bi+Qz+Fe–Ti+Ap+Zr
8	G019	Jiama	0.72	Pl+Am+Bi+Sani+Zr	Pl+Bi+Sani+Qz+Zr+Ap+Tit
8	G016	Jiama	0.69	Pl+Am+Bi+Sani+Zr+Fe–Ti	Pl+Bi+Sani+Qz+Zr+Ap
9	G025	Linzhi	0.60	Pl+Bi+Sani+Zr+Fe–Ti	Bi+Sani+Zr+Tit+Fe–Ti

Field no. refers to number of volcanic field in Fig. 1a. Am: amphibole; Ap: apatite; Bi: biotite; Cpx: clinopyroxene; Fe–Ti: Fe–Ti oxides; G: glass; Pl: plagioclase; Qz: quartz; Sani: sanidine; Tit: titanite; Zr: zircon.

Table 2
Major and trace element compositions of the Lhasa terrane adakites in south Tibet

Field no.:	1	2	2	3	4	5	6	7	8	8	9
Sample no.:	ZF09	GUO62	GUO51	GUO48	GUO37	G09	ZFG17	G006	G019	G016	G025
Locality:	Shiquanhe	Gegar	Gegar	Daggyai	Xigaze	Wuyu	Majiang	Nanmu	Jiama	Jiama	Linzhi
Longitude (E):	80.2	81.8	81.8	85.6	88.8	89.4	89.9	90.9	91.8	91.8	94.6
Latitude (N):	33.5	31.5	31.5	29.6	29.3	29.4	29.7	29.5	29.8	29.8	29.6
Age (Ma):	22.5	17.0	17.0	18.5	17.2	14.2	12.4	16.3	15.1	15.1	26.2
SiO_2	66.47	65.93	68.15	62.68	59.22	67.29	69.36	70.02	68.56	68.82	66.52
TiO_2	0.91	0.64	0.48	0.85	0.74	0.63	0.65	0.46	0.48	0.23	0.44
Al_2O_3	16.07	18.11	16.31	17.02	18.13	16.18	17.08	16.07	15.25	16.01	17.57
TFe_2O_3*	2.35	2.86	2.95	3.84	5.93	2.46	2.36	2.02	1.72	1.42	2.80
MnO	0.07	0.05	0.07	0.07	0.07	0.06	0.10	0.02	0.06	0.03	0.05
MgO	2.20	1.99	2.24	2.72	2.95	1.49	2.59	1.41	1.77	1.30	1.73
CaO	3.85	3.74	2.88	4.63	5.28	3.69	1.71	1.86	2.49	1.74	3.95
Na_2O	4.21	4.16	3.70	4.98	5.85	4.28	3.72	4.69	4.16	3.57	4.41
K_2O	3.48	2.24	2.83	2.79	1.68	3.70	2.15	3.31	5.37	6.77	2.38
P_2O_5	0.39	0.27	0.38	0.41	0.14	0.22	0.26	0.13	0.13	0.10	0.16
LOI	1.53	0.36	0.27	0.66	1.29	0.47	1.06	0.52	1.82	0.87	1.68
Total	99.78	99.52	100.47	99.54	99.91	99.76	99.63	99.89	100.04	99.93	99.64
Mg–no.	0.70	0.63	0.65	0.64	0.55	0.60	0.73	0.63	0.72	0.69	0.60
La	32.6	22.8	27.1	23.9	18.1	18.3	18.2	8.61	28.1	30.9	36.0
Ce	55.1	47.6	45.6	53.6	36.9	40.8	35.6	14.8	49.5	56.7	69.3
Pr	6.84	6.04	5.83	6.67	5.01	5.82	4.71	1.68	5.74	6.70	7.62
Nd	26.9	17.2	18.4	25.4	19.2	20.7	19.3	6.22	20.8	23.4	26.5
Sm	5.47	4.09	3.55	5.02	3.77	3.21	3.64	1.24	3.00	3.15	4.14
Eu	1.89	1.51	1.68	1.48	1.23	1.24	1.38	0.45	0.79	0.81	1.19
Gd	3.10	2.64	2.31	3.05	2.89	2.90	3.93	0.81	1.63	1.88	2.66
Tb	0.43	0.38	0.30	0.42	0.36	0.35	0.36	0.11	0.22	0.23	0.30
Dy	2.32	1.99	1.54	1.89	1.78	1.64	1.72	0.58	1.14	1.13	1.30
Ho	0.39	0.33	0.28	0.31	0.32	0.28	0.31	0.12	0.20	0.21	0.22
Er	0.91	0.76	0.70	0.80	0.82	0.72	0.78	0.33	0.49	0.56	0.59
Tm	0.13	0.11	0.11	0.11	0.12	0.10	0.11	0.05	0.07	0.08	0.09
Yb	0.88	0.76	0.73	0.67	0.71	0.65	0.68	0.33	0.44	0.48	0.56
Lu	0.13	0.12	0.11	0.10	0.09	0.09	0.11	0.05	0.06	0.06	0.08
Sc	5.95	5.10	4.88	5.27	6.75	5.05	4.82	8.44	3.95	3.04	6.46
V	41.9	58.5	45.1	70.6	72.1	38.6	57.5	55.5	42.2	34.8	48.0
Cr	59.0	78.7	52.2	81.9	89.0	46.9	57.9	46.8	42.7	55.0	56.8
Co	5.77	6.22	6.03	8.34	18.3	11.5	8.66	9.12	28.3	14.9	18.9
Ni	18.9	30.6	16.5	31.5	39.2	32.6	20.0	29.8	23.9	20.1	28.1
Cu	10.3	10.1	10.3	14.4	21.4	12.6	13.9	19.0	124	88.6	53.5
Zn	26.4	22.3	25.2	23.8	23.8	33.4	24.4	21.5	47.5	53.6	63.2
Ga	18.6	14.9	16.7	14.9	17.2	16.0	16.8	18.2	15.2	17.1	16.1
Rb	135	167	188	88.3	92.8	252	188	158	369	401	84.2
Sr	819	490	689	1024	1133	785	889	317	448	422	1003
Y	11.0	11.2	8.90	8.53	10.1	12.9	10.1	4.17	5.51	6.23	6.18
Zr	130	135	122	126	114	173	167	92.6	109	124	185
Nb	7.76	6.67	7.83	6.51	4.85	15.2	5.34	5.33	8.05	7.34	4.98
Ba	840	660	762	766	478	819	845	729	783	981	461
Hf	6.71	3.89	4.78	3.56	3.11	4.48	4.15	3.68	3.47	3.39	6.37
Ta	0.79	0.91	0.88	0.41	0.36	0.80	0.37	0.53	0.69	0.81	0.53
Pb	35.2	33.4	29.1	27.7	19.2	28.9	40.9	29.2	68.6	103	31.5
Th	16.5	16.7	21.4	10.1	3.14	42.3	21.6	12.6	16.4	29.8	10.4
U	13.3	20.3	15.3	2.12	0.91	3.67	4.11	1.82	5.37	8.46	2.14

Major element oxide contents are normalized to 100 wt.% on a volatile-free basis. Age (Ma) is average age of the volcanic field (or intrusive body) calculated from all of the age data in the published literature (Coulon et al., 1986; Yin et al., 1994; Miller et al., 1999; Williams et al., 2001; Chung et al., 2003; Williams et al., 2004; Hou et al., 2004). Field no. refers to number of the volcanic field (or intrusive body) in Fig. 1. Mg-no. = $Mg/(Mg+Fe^{2+})$, calculated assuming $Fe_2O_3/(FeO+Fe_2O_3)=0.20$. TFe_2O_3* means that total Fe is given as Fe_2O_3.

4. Analytical methods

Fresh samples, based on petrographic observations, were powdered in an agate mortar for major and trace element and Sr–Nd–Pb isotope analysis. Major elements were analyzed on fused glass discs with a Phillips PW1400 sequential X-ray fluorescence spectrometer (XRF) at the Institute of Geology and Geophysics, Chinese Academy of Sciences, Beijing, P. R. China (IGGCAS). The powders (1.2 g) were fused with $Li_2B_4O_7$ (6 g) in a CLAISSEFLUXER VI fusion furnace at 1050 °C for 20 min. The precision for major elements is better than 2% relative. The detailed analytical procedure follows that reported by Guo et al. (2005). Major element data are presented in Table 2.

Trace elements were determined using a Finnigan MAT inductively coupled plasma mass spectrometer (ICP-MS) at IGGCAS. Whole-rock powders (40 mg) were dissolved in distilled 1 ml HF and 0.5 ml HNO_3 in Savillex Teflon screw-cap capsules. The solutions were

Table 3
Sr, Nd and Pb isotope compositions of the Lhasa terrane adakites in south Tibet

Field no.:	1	2	2	3	4	5
Sample no.:	ZF09	GUO62	GUO51	GUO48	GUO37	G09
Locality:	Shiquanhe	Gegar	Gegar	Daggyai	Xigaze	Wuyu
Longitude (E):	80.2	81.8	81.8	85.6	88.8	89.4
Latitude (N):	33.5	31.5	31.5	29.6	29.3	29.4
Age (Ma):	22.5	17.0	17.0	18.5	17.2	14.2
$^{87}Sr/^{86}Sr \pm 2\sigma$	0.708124±9	0.707423±13	0.709188±11	0.706812±10	0.706639±11	0.706004±16
$^{143}Nd/^{144}Nd \pm 2\sigma$	0.512237±11	0.512354±10	0.512249±8	0.512147±13	0.512506±7	0.512588±9
$^{206}Pb/^{204}Pb$	18.403	18.256	18.311	18.513	18.510	18.314
$^{207}Pb/^{204}Pb$	15.609	15.580	15.612	15.640	15.609	15.578
$^{208}Pb/^{204}Pb$	38.314	38.267	38.308	39.084	38.423	38.156
$(^{87}Sr/^{86}Sr)_i$	0.707975	0.707192	0.709003	0.706748	0.706582	0.705821
$(^{143}Nd/^{144}Nd)_i$	0.512218	0.512337	0.512236	0.512132	0.512492	0.512579
$(^{206}Pb/^{204}Pb)_i$	18.320	18.156	18.224	18.499	18.502	18.297
$(^{207}Pb/^{204}Pb)_i$	15.605	15.575	15.608	15.639	15.609	15.577
$(^{208}Pb/^{204}Pb)_i$	38.280	38.240	38.268	39.062	38.414	38.090

Field no.:	6	7	8	8	9
Sample no.:	ZFG17	G006	G019	G016	G025
Locality:	Majiang	Nanmu	Jiama	Jiama	Linzhi
Longitude (E):	89.9	90.9	91.8	91.8	94.6
Latitude (N):	29.7	29.5	29.8	29.8	29.6
Age (Ma):	12.4	16.3	15.1	15.1	26.2
$^{87}Sr/^{86}Sr \pm 2\sigma$	0.704807±10	0.704911±15	0.708114±11	0.707937±14	0.705516±12
$^{143}Nd/^{144}Nd \pm 2\sigma$	0.512798±6	0.512604±10	0.512544±7	0.512511±8	0.512508±8
$^{206}Pb/^{204}Pb$	18.304	18.213	18.668	18.730	18.412
$^{207}Pb/^{204}Pb$	15.504	15.504	15.726	15.708	15.588
$^{208}Pb/^{204}Pb$	38.251	38.125	38.833	38.721	38.501
$(^{87}Sr/^{86}Sr)_i$	0.704702	0.704743	0.707617	0.707364	0.705428
$(^{143}Nd/^{144}Nd)_i$	0.512788	0.512591	0.512535	0.512503	0.512491
$(^{206}Pb/^{204}Pb)_i$	18.292	18.203	18.657	18.718	18.395
$(^{207}Pb/^{204}Pb)_i$	15.503	15.504	15.725	15.707	15.587
$(^{208}Pb/^{204}Pb)_i$	38.230	38.103	38.822	38.707	38.473

Field no. refers to the number of the volcanic field (or intrusive body) in Fig. 1. Age (Ma) is as in Table 2.
Chondritic uniform reservoir (CHUR) at the present day [$(^{87}Rb/^{86}Sr)_{CHUR}=0.0847$ (McCulloch and Black, 1984); $(^{87}Sr/^{86}Sr)_{CHUR}=0.7045$ (DePaolo, 1988); $(^{147}Sm/^{144}Nd)_{CHUR}=0.1967$ (Jacobsen and Wasserburg, 1980); $(^{143}Nd/^{144}Nd)_{CHUR}=0.512638$ (Goldstein et al., 1984)] was used for the calculations. $\lambda_{Rb}=1.42\times10^{-11}$ year^{-1} (Steiger and Jager, 1977); $\lambda_{Sm}=6.54\times10^{-12}$ year^{-1} (Lugmair and Marti, 1978); $\lambda_{U238}=0.155125\times10^{-9}$ year^{-1}, $\lambda_{U235}=0.98485\times10^{-9}$ year^{-1} and $\lambda_{Th232}=0.049475\times10^{-9}$ year^{-1} (Steiger and Jager, 1977).
$(^{207}Pb/^{204}Pb)_{NHRL}=0.1084\times(^{206}Pb/^{204}Pb)_i+13.491$ (Hart, 1984); $(^{208}Pb/^{204}Pb)_{NHRL}=1.209\times(^{206}Pb/^{204}Pb)_i+15.627$ (Hart, 1984).
Initial Sr, Nd and Pb isotope ratios were obtained by using the average age of the volcanic field (or intrusive body).

heated at 170 °C for 10 days, dried and redissolved in 2 ml HNO_3 in the capsules. Finally, the solutions were diluted in 1% HNO_3 to 50 ml before analysis. A blank solution was analyzed; procedural blanks were <50 ng for the trace elements listed in Table 2. The detailed analytical procedures follow those of Jin and Zhu (2000) and Guo et al. (2005).

Sr–Nd isotope analyses were performed on a VG354 mass spectrometer at IGGCAS. Sample powders (60 mg) were spiked with mixed isotope tracers, then dissolved with a mixed acid (HF: $HClO_4$=3:1) in Teflon capsules for 7 days. Rb, Sr, Sm and Nd were separated in solution using AG50W×8 (H^+) cationic ion-exchange resin columns. The international standard NBS987 gave $^{87}Sr/^{86}Sr$= 0.710254±16 (n=8, 2 sigma) and standard NBS607 gave $^{87}Sr/^{86}Sr$=1.20032±30 (n=12). The La Jolla standard yielded $^{143}Nd/^{144}Nd$=0.511862±7 (n=12) and standard BCR-1 yielded $^{143}Nd/^{144}Nd$=0.512626±9 (n=12). The mass fractionation corrections for Sr and Nd isotopic ratios were based on $^{86}Sr/^{88}Sr$=0.1194 and $^{146}Nd/^{144}Nd$=0.7219, respectively. The whole procedure blank is less than 2×10^{-10} g for Rb–Sr isotopic analysis and 5×10^{-11} g for Sm–Nd analysis. Analytical errors for Sr and Nd isotopic ratios are given as 2σ in Table 3.

150 mg whole-rock powder was dissolved in Teflon capsules using concentrated HF at 120 °C for 7 days. Pb was separated and purified using AG1×8 anionic ion-exchange columns. The procedure blank is less than 1 ng. Pb isotopic ratios were measured with a VG354 mass spectrometer at IGGCAS. The standard NBS981 yielded $^{204}Pb/^{206}Pb$=0.059003±0.000084 (n=6), $^{207}Pb/^{206}Pb$=0.91449±0.00017 (n=6) and $^{208}Pb/^{206}Pb$= 2.16691±0.00097 (n=6). The average 2σ uncertainty for $^{206}Pb/^{204}Pb$, $^{207}Pb/^{204}Pb$ and $^{208}Pb/^{204}Pb$ is 0.7%, 0.3% and 0.6% per a.m.u. (atomic mass unit), respectively. The Pb isotope data are presented in Table 3. Detailed analytical procedures for the Sr–Nd–Pb isotope measurements follow those of Guo et al. (2005).

5. Results

All of the studied samples have high SiO_2 (59–70 wt.%), Al_2O_3 (15–18 wt.%) and K_2O (1.7–6.8 wt.%) (Fig. 2), and low MgO (1.3 to 3.0 wt.%), Y (4.2–12.9 ppm; Fig. 3) and heavy rare earth element (HREE) concentrations (e.g. Yb=0.3–0.9 ppm and Yb_N=2–5 (the subscript 'N' denotes that the concentration is normalized to the chondritic abundance)). These characteristics, together with the high Sr contents (317–1133 ppm) and Sr/Y ratios (44–162) (Fig. 3), indicate that the samples can be classified as adakites as defined by Defant and Drummond (1990, 1993) and Martin (1999), except for their relatively high

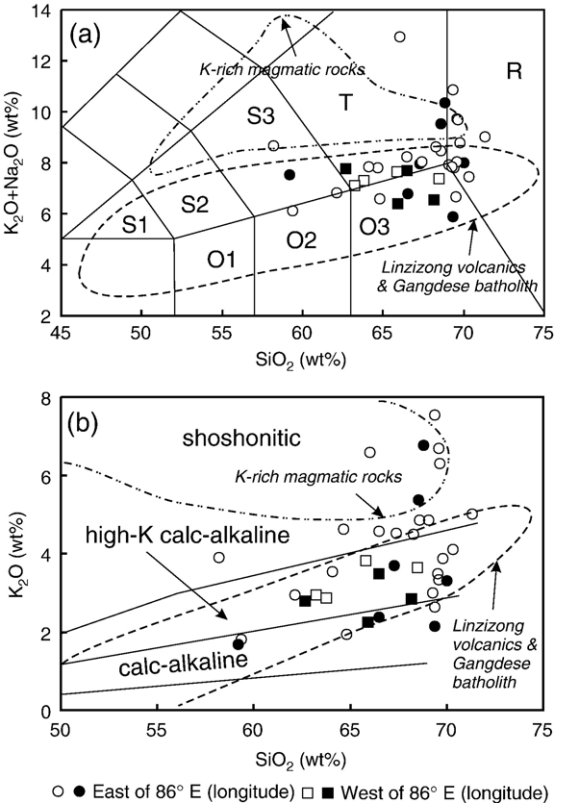

Fig. 2. (a) K_2O+Na_2O (wt.%) vs SiO_2 (wt.%) for the adakites in south Tibet. All data plotted have been recalculated to 100 wt.% on a volatile-free basis. Classification boundaries are from Le Bas et al. (1986) and Le Maitre et al. (1989). Filled and open symbols represent, respectively, data for adakites from south Tibet from this study and previously published literature (Turner et al., 1996; Miller et al., 1999; Williams et al., 2001; Zhao et al., 2001; Chung et al., 2003; Hou et al., 2004; Qu et al., 2004; Williams et al., 2004). Rock types shown by letters are as follows. S1: trachybasalt; S2: basaltic trachyandesite; S3: trachyandesite; T: trachyte; R: rhyolite; O1: basaltic andesite; O2: andesite; O3: dacite. The dot-dashed line denotes the field of K-rich magmatic rocks in the Lhasa terrane (Miller et al., 1999; Williams et al., 2001; Ding et al., 2003; Nomade et al., 2004; Williams et al., 2004). The dashed line represents field of the Linzizong volcanic rocks and the Gangdese batholith in the Lhasa terrane of the southern Tibetan Plateau (Zhang, 1996; Jiang et al., 1999; Song, 1999; Wu et al., 2005). (b) K_2O (wt.%) vs SiO_2 (wt.%) diagram for the same samples plotted in (a). Data have been normalized to 100 wt.% volatile-free as indicated in Table 2. The dividing lines show the classification boundaries from Rickwood (1989). Data sources and symbols are as in (a).

contents of K_2O and high Mg-numbers (0.55–0.73). The studied samples have flat heavy REE patterns (Fig. 4). They show strong enrichment in large ion lithophile elements (LILE) relative to high field strength elements (HFSE) and pronounced negative Nb–Ta anomalies and positive K and Pb anomalies in MORB-normalised incompatible element patterns (Fig. 5). The analysed samples have high $(^{87}Sr/^{86}Sr)_i$ (0.704702–0.709003) and

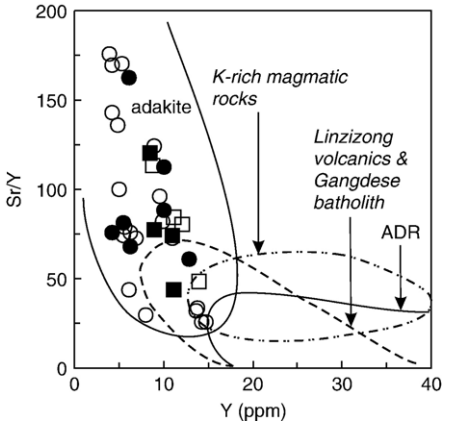

Fig. 3. Sr/Y vs Y (ppm). The fields for adakite and ADR (normal island-arc andesite–dacite–rhyolite) are based on the work of Defant and Drummond (1990, 1993) and Castillo et al. (1999). Symbols are as in Fig. 2.

low ($^{143}Nd/^{144}Nd)_i$ (0.512132–0.512788) relative to Bulk Earth values, and high ($^{207}Pb/^{204}Pb)_i$ (15.5–15.7) and ($^{208}Pb/^{204}Pb)_i$ (38.1–39.1) at a given ($^{206}Pb/^{204}Pb)_i$ (18.2–18.7) compared to the Northern Hemisphere Reference Line (NHRL; Hart, 1984) (Fig. 6).

Whilst the adakites from east and west of 86° E are compositionally similar, those to the east have higher contents of K_2O (Fig. 2b), light rare earth elements (LREE) (Fig. 4b) and LILE (Fig. 5b), higher Sr/Y ratios (Fig. 3) and less radiogenic Sr and more radiogenic Nd isotopic compositions (Fig. 6a), suggesting a decoupling between the incompatible element and Sr–Nd isotopic signatures. The adakites to the west of 86° E have lower Pb isotope ratios than those to the east of 86° E (Fig. 6c, d). In the $^{207}Pb/^{204}Pb$ and $^{208}Pb/^{204}Pb$ vs $^{206}Pb/^{204}Pb$ diagrams (Fig. 6c and d) the adakites overlap the field of Indian MORB, defining a positive array which extends towards the field of Global Subducting Sediment (GLOSS; Plank and Langmuir, 1998).

6. Discussion

The major and trace element and Sr–Nd–Pb isotope characteristics of the Tibetan adakites can be used to provide important constraints on the nature of their source region and the geodynamic evolution of south Tibet following the India–Asia collision.

6.1. Nature of the source region of the adakitic magmas

The MORB-normalised incompatible element patterns of the adakites (Fig. 5) exhibit strong enrichments in LILE and negative Ta–Nb anomalies, suggesting affinities with magmas generated in subduction-related tectonic settings. Previous studies (e.g. Elburg et al., 2002; Guo et al., 2005) have shown that there are two types of component – partial melts of subducted sediment and slab-derived fluids – which may metasomatise and enrich the source region of subduction-related magmas. Slab-derived fluids are characterized by high contents of Ba, Rb, Sr, U and Pb, whereas partial melts of subducted sediment have high concentrations of Th and LREE (Hawkesworth et al., 1997a, 1997b; Guo et al., 2005, 2006). On this basis, the linear trend of the adakites in a plot of Th/Yb vs Th/Sm (Fig. 7a) could be interpreted in terms of two-component mixing between N-MORB (or a partial melt thereof) and a partial melt of subducted

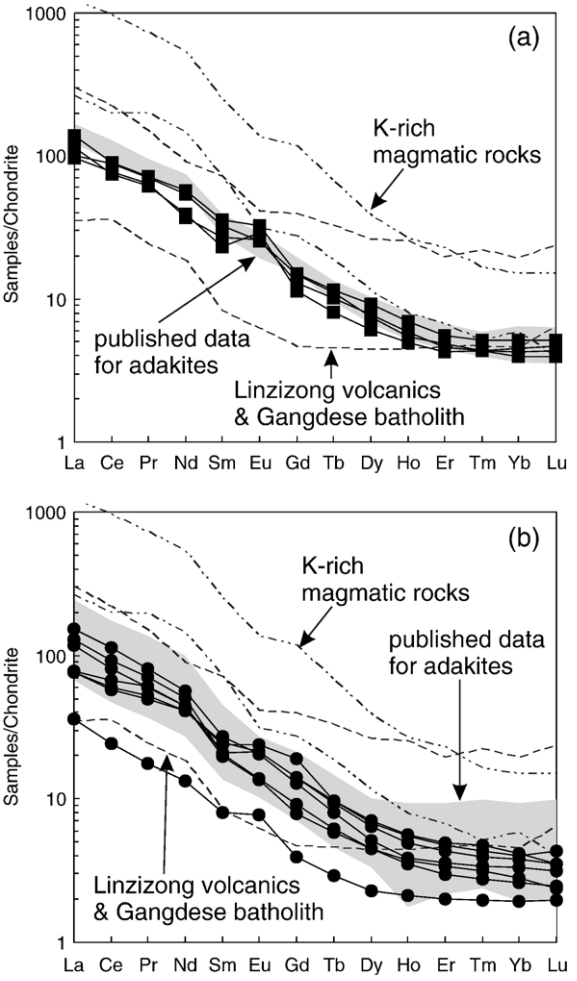

Fig. 4. Chondrite-normalised rare earth element diagrams; normalization factors are from Sun and McDonough (1989). (a) Adakites to the west of 86° E. (b) Adakites to the east of 86° E. The grey field denotes previously published data for adakites in the Lhasa terrane of the southern Tibetan Plateau (Turner et al., 1996; Miller et al., 1999; Williams et al., 2001; Zhao et al., 2001; Chung et al., 2003; Hou et al., 2004; Qu et al., 2004; Williams et al., 2004). Symbols are as in Fig. 2.

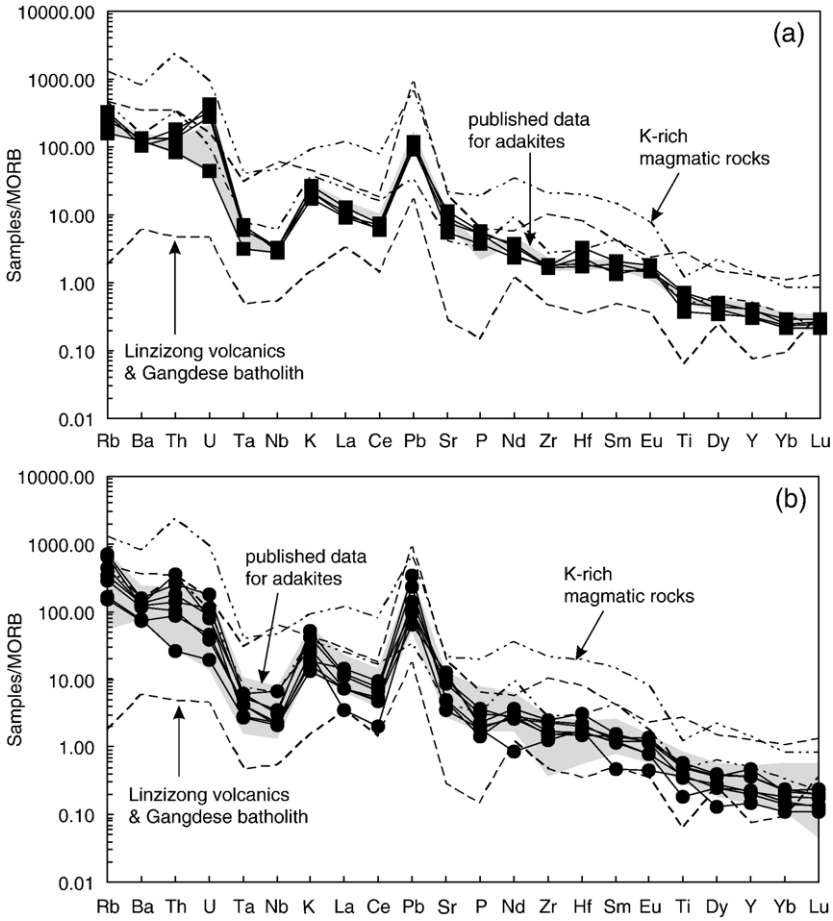

Fig. 5. MORB-normalised incompatible trace element diagrams; normalization factors are from Pearce and Parkinson (1993). (a) Adakites to the west of 86° E. (b) Adakites to the east of 86° E. The grey field represents previously published data for adakites in the Lhasa terrane of the southern Tibetan Plateau (Turner et al., 1996; Miller et al., 1999; Williams et al., 2001; Zhao et al., 2001; Chung et al., 2003; Hou et al., 2004; Qu et al., 2004; Williams et al., 2004). Symbols are as in Fig. 2.

sediment. This inference is also consistent with the linear trends between Indian MORB and GLOSS (Plank and Langmuir, 1998) defined by the adakites in the Sr–Nd–Pb isotope diagrams (Fig. 6). Two-component mixing is also supported by the flat trend of the adakite data in a plot of Ba/Th vs $(^{87}Sr/^{86}Sr)_i$ (Fig. 7b). The Sr–Nd–Pb isotope characteristics of the adakites also overlap with those of the Late Cretaceous–Early Tertiary Linzizong volcanics and Gangdese granitoid batholith which together form part of a subduction-related continental margin arc within the Lhasa terrane (Fig. 8).

The low HREE concentrations ($Yb_N < 6$) and flat normalized HREE patterns of the adakites (Fig. 4) strongly suggest the presence of garnet as a residual phase in their source. Moreover, the relative depletion of Ba with respect to Rb in the MORB-normalised incompatible element patterns (Fig. 5) suggests that amphibole might also be a residual phase, reflecting its higher partition coefficient for Ba than Rb (Green, 1994; Foley et al., 1996). The relatively low Ba/Th ratios in the adakites (Fig. 7b) are also consistent with the presence of residual amphibole in the source due to the preferential retention of Ba in amphibole.

6.2. Petrogenesis of the adakites in south Tibet

Geochemical (e.g. Kay, 1978; Defant and Drummond, 1990; Kay et al., 1993; Yogodzinski et al., 1994, 1995; Garrison and Davidson, 2003), experimental (e.g. Sen and Dunn, 1994; Rapp and Watson, 1995; Martin, 1999; Rapp et al., 1999) and numerical simulation (e.g. Petford and Gallagher, 2001; Annen and Sparks, 2002) studies suggest that partial melting of metabasic igneous rocks in the eclogite to amphibolite facies, either in the thickened lower crust or subducted oceanic crust, can produce melts with the geochemical characteristics of

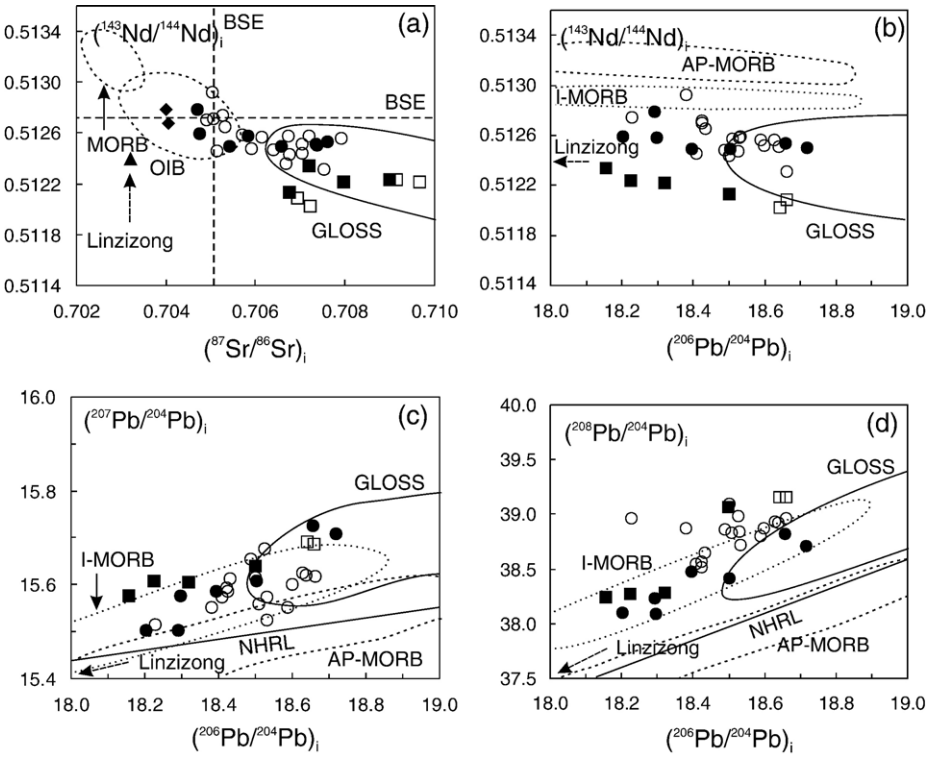

Fig. 6. (a) $(^{143}Nd/^{144}Nd)_i$ vs $(^{87}Sr/^{86}Sr)_i$. (b) $(^{143}Nd/^{144}Nd)_i$ vs $(^{206}Pb/^{204}Pb)_i$. (c) $(^{207}Pb/^{204}Pb)_i$ vs $(^{206}Pb/^{204}Pb)_i$. (d) $(^{208}Pb/^{204}Pb)_i$ vs $(^{206}Pb/^{204}Pb)_i$. Field for Central Indian MORB (I-MORB) is from Mahoney et al. (1989) and Hofmann (1997). Field for Atlantic+Pacific MORB (AP-MORB) is from White et al. (1987) and Hofmann (1997). The solid line outlines the field of Global Subducting Sediment (GLOSS; Plank and Langmuir, 1998). The NHRL (Northern Hemisphere Reference Line; Hart, 1984), and MORB and OIB fields (Wilson, 1989; Hofmann, 1997) are shown for reference. BSE is Bulk Silicate Earth. The filled triangle indicated by an arrow with a dashed line in (a) denotes Linzizong basalt (Zhang, 1996). The filled rhombs in (a) represent Gangdese batholith gabbros (Jiang et al., 1999). The direction indicated by an arrow with a dashed line in (b–d) denotes the Linzizong basalt (Zhang, 1996). Symbols are as in Fig. 2.

adakites. Additionally, adakite-like melt compositions can also be produced by combined assimilation and fractional crystallization (AFC) of mantle-derived magmas during their transit through the continental crust (Castillo et al., 1999; Castillo, 2006).

We first consider the possibility that the south Tibet adakites originated by partial melting of subducted oceanic crust. Significant differences between the Sr–Nd isotope compositions of Neotethyan MORB (oceanic crust) (Hou et al., 2004) and the adakites (Fig. 8a) are inconsistent with a simple model of slab melting. However, the Sr–Nd–Pb isotope compositions of the adakites could be consistent with mixing of melts derived from the subducted oceanic crust with partial melts of subducted oceanic sediment (Figs. 6 and 7).

A second possibility is that the south Tibet adakites formed by AFC processes similar to the model proposed by Castillo et al. (1999) to explain the petrogenesis of adakitic magmas on Camiguin Island in the Philippines. There is indeed a close spatial and temporal association between the occurrence of adakites and mafic, potassic–ultrapotassic, igneous rocks in the Lhasa terrane. However the potassic–ultrapotassic magmatic rocks have much higher $^{87}Sr/^{86}Sr$, LILE and K_2O contents, and lower $^{143}Nd/^{144}Nd$ compared to the adakites (Figs. 5 and 8) which would require a rather unusual AFC trajectory. Energy-constrained assimilation-fractional crystallization (EC-AFC) model calculations (Bohrson and Spera, 2001; Guo et al., 2006) confirm that the south Tibet adakites could not be produced by fractional crystallization of contemporaneous, potassic–ultrapotassic, mafic magmas combined with assimilation of andesitic lower crust, whose composition is approximated based on that of the average composition of the Linzizong volcanics–Gangdese batholith in the Lhasa terrane. If the south Tibet adakites were formed by AFC processes, we would predict that their $^{87}Sr/^{86}Sr$ ratios should be closer to those of the mafic, K-rich magmatic rocks, than to the Linzizong volcanics and Gangdese batholith (Fig. 8a), because the Sr contents of the mafic, K-rich magmatic rocks (Miller et al.,

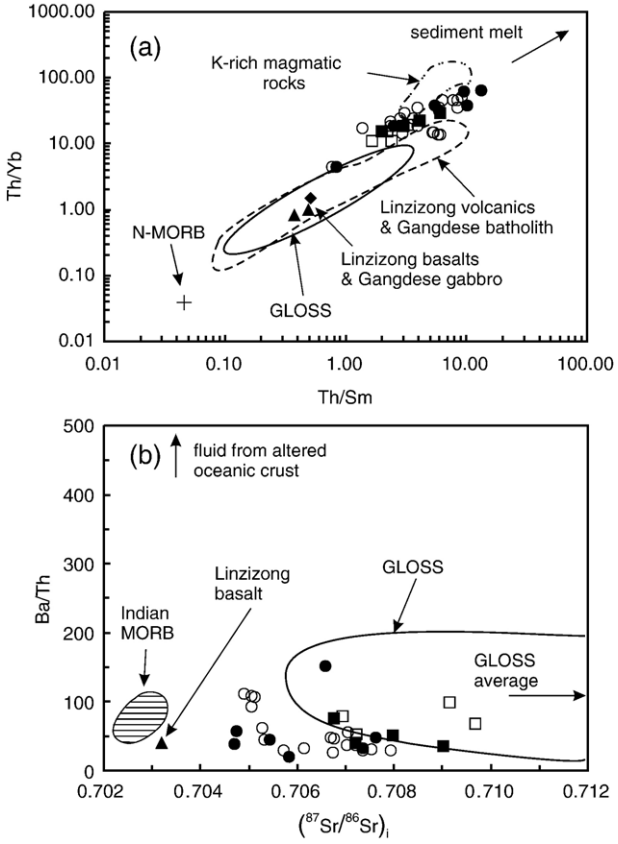

Fig. 7. (a) Th/Yb vs Th/Sm. (b) Ba/Th vs $(^{87}Sr/^{86}Sr)_i$. Data for N-MORB, Indian MORB and GLOSS are taken from Sun and McDonough (1989), Rehkämper and Hofmann (1997) and Plank and Langmuir (1998), respectively. The filled triangles denote Linzizong basalts (Zhang, 1996). The filled rhomb in (a) represents a Gangdese batholith gabbro (Jiang et al., 1999). The composition of the fluid derived from subducted altered oceanic crust in (b) is from Turner et al. (1997). Symbols are as in Fig. 2.

1999; Williams et al., 2001; Ding et al., 2003; Williams et al., 2004) are much higher than those of the Linzizong volcanics and Gangdese batholith (Zhang, 1996; Jiang et al., 1999; Song, 1999; Wu et al., 2005). Thus, we do not consider that the south Tibet adakites could have originated by crustal AFC processes.

Finally, we evaluate the possibility that the south Tibet adakites originated by partial melting of the continental crust of the Lhasa terrane which is presently more than 70 km thick (Owens and Zandt, 1997). Crustal thickening most likely occurred during the Mesozoic–Early Tertiary phase of subduction-related magmatism within the Lhasa terrane (e.g. Scharer et al., 1984; Coulon et al., 1986; Zhang, 1996; Jiang et al., 1999; Mo et al., 2003) (Fig. 1). The lower crust is likely to be a heterogeneous mixture of mafic and more evolved igneous rocks which crystallized from subduction-related magmas undergoing AFC processes (cf. Annen et al., 2006). We propose that it is composed of meta-basic to meta-intermediate igneous rocks in the garnet–amphibolite to granulite facies based on the data presented by Garrido et al. (2006) for the exhumed lower crust of the Kohistan arc further to the west. The evolution of the lower crust of the Lhasa terrane during the subduction-related magmatic phase was most probably dominated by AFC processes involving primitive mafic magmas similar to the Linzizong basalts or Gangdese gabbros and the local lower crust. The differences in Sr–Nd–Pb isotope compositions (Fig. 8) between the Linzizong basalts (and Gangdese gabbros) (Zhang, 1996; Jiang et al., 1999; Mo et al., 2003; Huang et al., 2004) and the adakites, however, indicates that petrogenesis of the adakites is not easily explained by partial melting of mafic lower crustal rocks similar in composition to the mafic end-members of the Linzizong–Gangdese subduction-related magmatic suite. The overlapping Sr–Nd–Pb isotope compositions (Fig. 8) of the Linzizong andesites and Gangdese batholith diorites (Zhang, 1996; Jiang et al., 1999; Mo et al., 2003; Huang et al., 2004) and the adakites suggest, instead, that the

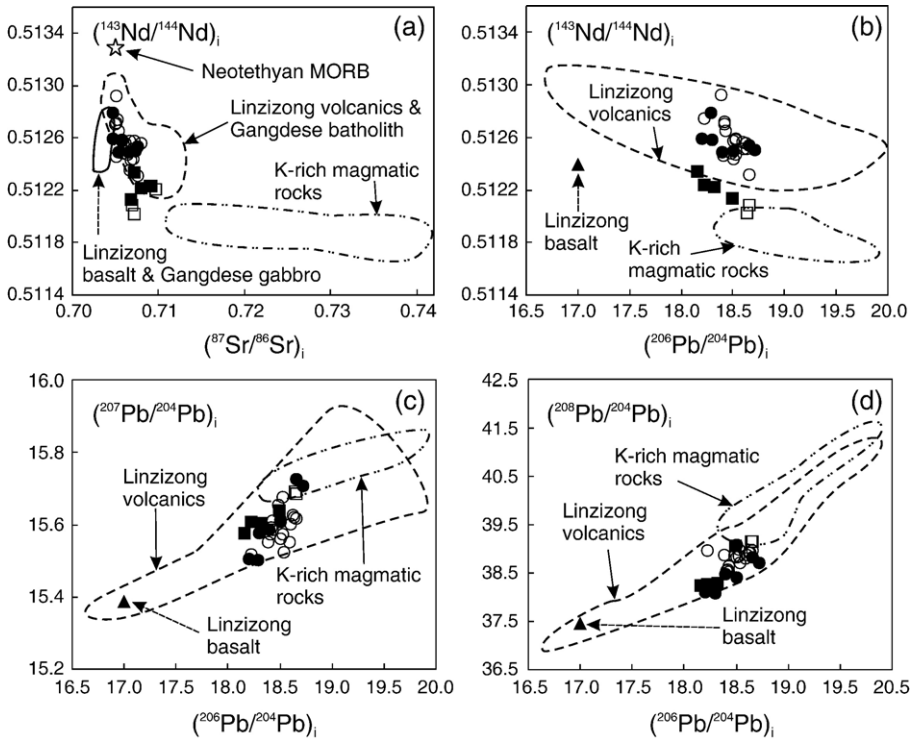

Fig. 8. (a) $(^{143}Nd/^{144}Nd)_i$ vs $(^{87}Sr/^{86}Sr)_i$. (b) $(^{143}Nd/^{144}Nd)_i$ vs $(^{206}Pb/^{204}Pb)_i$. (c) $(^{207}Pb/^{204}Pb)_i$ vs $(^{206}Pb/^{204}Pb)_i$. (d) $(^{208}Pb/^{204}Pb)_i$ vs $(^{206}Pb/^{204}Pb)_i$. The field for the Linzizong volcanics (Zhang, 1996; Mo et al., 2003; Huang et al., 2004) and Gangdese batholith (Jiang et al., 1999) are indicated. Linzizong basalt (Zhang, 1996) and Gangdese gabbro (Jiang et al., 1999) in (a) represent the primitive, mafic end-member of the Linzizong and Gangdese magmatic rocks. Data for the K-rich magmatic rocks are from Miller et al. (1999), Williams et al. (2001, 2004), Ding et al. (2003) and Nomade et al. (2004). The filled triangles in (b–d) denote Linzizong basalt (Zhang, 1996). The open star in (a) represents the Neotethyan basaltic ocean crust (Hou et al., 2004). Symbols are as in Fig. 2.

adakites could be derived by partial melting of more evolved subduction-related magmatic rocks which had crystallized at depth within the lower crust. The overlapping major and trace element characteristics of the Linzizong andesites and Gangdese batholith diorites (Zhang, 1996; Jiang et al., 1999; Song, 1999; Wu et al., 2005) and the southern Tibetan adakites (Figs. 2, 4, 5) support this inference.

In order to partially melt the lower crust of the Lhasa terrane we clearly need a heat source. This could be provided by the migration of the contemporaneous (25.4–8.2 Ma), mafic, potassic–ultrapotassic magmas, derived from lithospheric (e.g. Coulon et al., 1986; Miller et al., 1999; Williams et al., 2001; Chung et al., 2003; Ding et al., 2003; Williams et al., 2004; Fig. 1) or asthenospheric mantle sources (Guo et al., 2006).These potassic–ultrapotassic magmas were generated after a period of magmatic quiescence from 40–26 Ma (Maheo et al., 2002) following the cessation of subduction-related magmatism.

The Nd isotope compositions of the adakites to the west of 86° E are similar to those of the contemporaneous, K-rich, magmatic rocks whereas those to the east of 86° E have higher $^{143}Nd/^{144}Nd$ ratios (Fig. 8a and b). This suggests that the adakites to the west of 86° E, with lower $^{143}Nd/^{144}Nd$ ratios, might originate by mixing between mafic K-rich magmas (which could provide the heat source for crustal melting) and partial melts of Linzizong-like andesitic (and Gangdese-like dioritic) lower crust, while the adakites to the east of 86° E, with higher $^{143}Nd/^{144}Nd$ ratios, could be predominantly partial melts of the lower crust. Such mixing might explain the higher K_2O (1.7–6.8 wt.%) and MgO contents (1.3–3.0 wt.%) and Mg-numbers (0.55–0.73) of the adakites in south Tibet (Table 2) compared to experimentally produced adakitic melts (Martin, 1999; Rapp et al., 1999). The narrow range of variation, particularly in $^{206}Pb/^{204}Pb$, in the Pb isotope plots (Fig. 8c and d) makes it difficult to identify distinct mixing end-members; additionally there is no obvious correlation between Pb isotope composition and geographic location (i.e. east or west of 86° E). The $^{206}Pb/^{204}Pb$, $^{207}Pb/^{204}Pb$ and $^{208}Pb/^{204}Pb$ ratios of the K-rich magmatic rocks are higher than those of adakites (Fig. 8c and d) suggesting that the proportion of K-rich melt in the adakitic magma source must be quite small.

6.3. Trace element modelling

To evaluate whether partial melting of subducted oceanic crust or subduction-modified lower continental crust provides the best explanation for the petrogenesis of the adakites we have attempted to simulate quantitatively the trace element characteristics of the Lhasa terrane adakites using a non-modal batch melting model (Wilson, 1989).

As noted earlier, the trace element characteristics of the adakites provide some useful constraints on the mineralogy of their source. The negative Ta–Nb, P and Ti anomalies in their MORB-normalised incompatible element patterns (Fig. 5) are consistent with the presence of residual rutile and apatite in the source region. Garnet and amphibole are also likely based on the low HREE concentrations (Fig. 4) and negative Ba anomalies (Fig. 5). The lack of negative Eu anomalies in the chondrite normalized REE patterns (Fig. 4) indicates that the melting residue was plagioclase-free.

6.3.1. Partial melting of subducted oceanic crust

To model partial melting of subducted oceanic crust and its cover of sediment we used a normal MORB (i.e. N-MORB; Pearce and Parkinson, 1993) composition to represent that of the subducted Neotethyan basaltic oceanic crust and the average Global Subducting Sediment (GLOSS; Plank and Langmuir, 1998) composition to approximate that of the overlying sediment. Based on the trace element characteristics of the adakites, experimental studies of metabasalt melting (e.g. Sen and Dunn, 1994; Rapp and Watson, 1995) and petrogenetic simulations (e.g. Defant et al., 1991; Tsuchiya and Kanisawa, 1994; Yogodzinski et al., 1994, 1995; Sajona et al., 2000), we constrained the original mineral assemblage in the subducted slab (basaltic oceanic crust plus its overlying sediment) to be garnet+clinopyroxene+hornblende+rutile+apatite. Since we do not know the proportions of these phases precisely, we performed a series of iterative calculations, following the approach of Guo et al. (2005, 2006), progressively changing the proportions of each mineral from 0% to 80% until we obtained the best fit to the MORB-normalised incompatible element patterns of the adakites. We assumed the following mineral melting mode (i.e. the proportion of the mineral phases entering the melt): apatite (0.15), clinopyroxene (0.30), garnet (−0.10), amphibole (0.60) and rutile (0.05), based on the experimental studies of Sen and Dunn (1994) and Rapp and Watson (1995) and the modeling approach of Guo et al. (2005, 2006). The mineral-melt trace element partition coefficients (Table 4) used in the calculations were taken from Green (1994), Williams et al. (2004) and the GERM website (http://www.earthref.org/) for dacitic and andesitic melt compositions.

The results of the calculations suggest that the original mineral proportions in the subducted slab could have been different to the east and west of 86° E; the modal mineralogy to the east of 86° E involves garnet (0.15), clinopyroxene (0.65), amphibole (0.18), rutile (0.01) and apatite (0.01), while that to the west of 86° E involves garnet (0.08), clinopyroxene (0.755), amphibole (0.15), rutile (0.005) and apatite (0.01). The best fit model results (Table 5, Fig. 9a and b) suggest that a melt with trace element characteristics similar to those of the Lhasa terrane adakites could be generated by ~5% slab melting with ~20% subducted sediment in the slab. However, the V, Cr and Ni contents of the model slab melts (not shown) are much lower than those of the adakites, requiring that the slab melts would have to interact with the overlying mantle

Table 4
Mineral-melt partition coefficients for andesitic–dacitic melts

Mineral	Rb	Ba	Th	U	Ta	Nb	K	La	Ce	Pb	Sr
Amphibole	0.18	0.92	0.45	0.05	0.21	1.5	1.15	0.435	0.63	0.53	0.49
Apatite	0.4	0.3	1.6	1.82	142			21.7	16.6	0.03	8
Cpx	0.1	0.135	0.01	0.17	0.04	0.6	0.0366	0.28	0.48	0.85	0.37
Garnet	0.00851	0.0172	0.00137	0.00588	0.22	0.0538	0.0198	0.37	0.53	0.00012	0.0154
Rutile	0.0076	0.0137	0.54		44.7	29.8			0.73		0.518

Mineral	P	Nd	Zr	Hf	Sm	Eu	Ti	Dy	Y	Yb	Lu
Amphibole	0.5	1.24	0.93	0.76	0.66	0.358	3.66	1.77	0.017	1.31	4.025
Apatite	100	21	2	0.4	20.7	14.5		16.9		9.4	7.9
Cpx	0.05		0.5	0.2	1.6	1.65	0.78	2.675	5.15	1.4	1.4
Garnet	0.15	0.81	0.4	3.3	5.5	1.37	5.6	28.6	4.66	26	23.5
Rutile	0.05	0.277	4.76	4.98		0.00037	11	0.00076	0.076	0.0093	0.0124

Blank denotes no data are available. Cpx: clinopyroxene.
Data source: Green (1994), Williams et al. (2004), GERM (Geochemical Earth Reference Model) home page, http://www.earthref.org/.

Table 5
Results of the trace element modelling

(a) Slab melting model

Element	Rb	Ba	Th	U	Ta	Nb	K_2O	La	Ce	Pb	Sr
West[a]	80.68	610.33	12.65	2.00	0.39	4.85	2.36	19.64	30.68	5.68	339.09
East[b]	83.20	577.98	11.19	2.19	0.28	4.11	2.06	19.18	30.19	6.30	357.14
Average adakite (west)	144.58	757.00	16.18	12.76	0.75	7.19	2.84	26.60	50.48	31.35	755.50
Average adakite (east)	220.71	728.00	19.46	3.78	0.58	7.30	3.62	22.60	43.37	45.90	713.86
Element	P_2O_5	Nd	Zr	Hf	Sm	Eu	TiO_2	Dy	Y	Yb	Lu
West[a]	0.23	35.03	146.27	4.20	1.78	0.74	0.73	0.98	6.66	0.86	0.12
East[b]	0.22	27.01	139.74	2.92	1.58	0.77	0.56	0.71	7.01	0.58	0.09
Average adakite (west)	0.36	21.98	128.25	4.74	4.53	1.64	0.72	1.94	9.91	0.76	0.12
Average adakite (east)	0.16	19.45	137.80	4.09	3.16	1.01	0.52	1.33	7.88	0.55	0.08

(b) Lower crustal melting model

Element	Rb	Ba	Th	U	Ta	Nb	K_2O	La	Ce	Pb	Sr
West[a]	156.98	552.68	13.69	7.45	0.53	6.07	1.86	39.39	66.13	64.65	1246.39
East[b]	189.89	568.78	14.63	8.97	0.27	5.71	1.90	31.88	57.84	66.79	1176.04
Lower crust[c]	36.34	354.87	4.89	1.42	0.62	7.60	1.36	21.43	46.05	42.56	655.67
Element	P_2O_5	Nd	Zr	Hf	Sm	Eu	TiO_2	Dy	Y	Yb	Lu
West[a]	0.31	25.14	146.33	4.71	3.92	1.36	0.44	1.33	9.85	0.85	0.10
East[b]	0.17	21.73	144.49	4.88	3.57	1.25	0.43	1.32	9.82	0.88	0.10
Lower crust[c]	0.27	22.63	118.23	3.30	4.85	1.27	1.12	3.80	18.69	1.78	0.34

Contents of K_2O, P_2O_5 and TiO_2 are shown in wt.%; other elements are in ppm.
The expression and approach of the non-modal batch partial melting model follow that of Guo et al. (2005, 2006).
[a] Model trace element contents in the adakites to the west of 86° E.
[b] Model trace element contents in the adakites to the east of 86° E.
[c] Assumed lower crust compositions (average) based on Zhang (1996), Jiang et al. (1999), Song (1999) and Wu et al. (2005). More detailed discussions see the main text.

(asthenosphere or lithosphere) in a mantle AFC-type process in order to provide a viable petrogenetic model.

6.3.2. *Partial melting of subduction-modified lower continental crust*

To model partial melting of subduction-modified lower crust we used the average composition of the more mafic (SiO_2 < 60 wt.%) Linzizong volcanics and Gangdese batholith (Zhang, 1996; Jiang et al., 1999; Song, 1999; Wu et al., 2005) to represent that of the lower crust in the Lhasa terrane (Table 5). As in the model for partial melting of subducted oceanic crust we adopted a mineral assemblage involving garnet + clinopyroxene + amphibole + rutile + apatite. This mineral assemblage is consistent with that of the exhumed mafic lower crust in the Kohistan arc (Garrido et al., 2006) which includes a range of rock types. Based on the observations of Garrido et al. (2006) we selected three feldspar-free, mafic, meta-igneous crustal rock types (garnet-clinopyroxene hornblendite (garnet 2%, clinopyroxene 35%, amphibole 60%, rutile 1% and apatite 2%), garnet-rich hornblende pyroxenite (garnet 10%, clinopyroxene 57%, amphibole 30%, rutile 1% and apatite 2%) and garnet-poor hornblende pyroxenite (garnet 1%, clinopyroxene 66%, amphibole 30%, rutile 1% and apatite 2%)) as potential source rocks of the adakites, adopting a non-modal batch melting model following the approach of Guo et al. (2005, 2006). We used the same mineral melting mode as in the model for partial melting of subducted oceanic crust, based on available experimental studies (Sen and Dunn, 1994; Rapp and Watson, 1995) and the modeling approach (Guo et al., 2005, 2006). The mineral-melt trace element partition coefficients are given in Table 4.

The best fit to the MORB-normalised incompatible element patterns of the southern Tibetan adakites (Table 5, Fig. 9c and d) was obtained when the proportions of the above minerals in the model lower crust were similar to those of the garnet-clinopyroxene hornblendite. Thus, we propose that the Lhasa terrane adakites could have been derived by partial melting of a garnet–clinopyroxene hornblendite protolith with 2% garnet, 35% clinopyroxene, 60% amphibole, 1% rutile and 2% apatite. The calculated degree of partial melting of the lower crust is ~10% to the west of 86° E and ~5% to the east of 86° E. This suggests that the differences in the LILE contents of the adakites to the east and west of 86° E could have been caused mainly by variable degrees of partial melting of the lower crust.

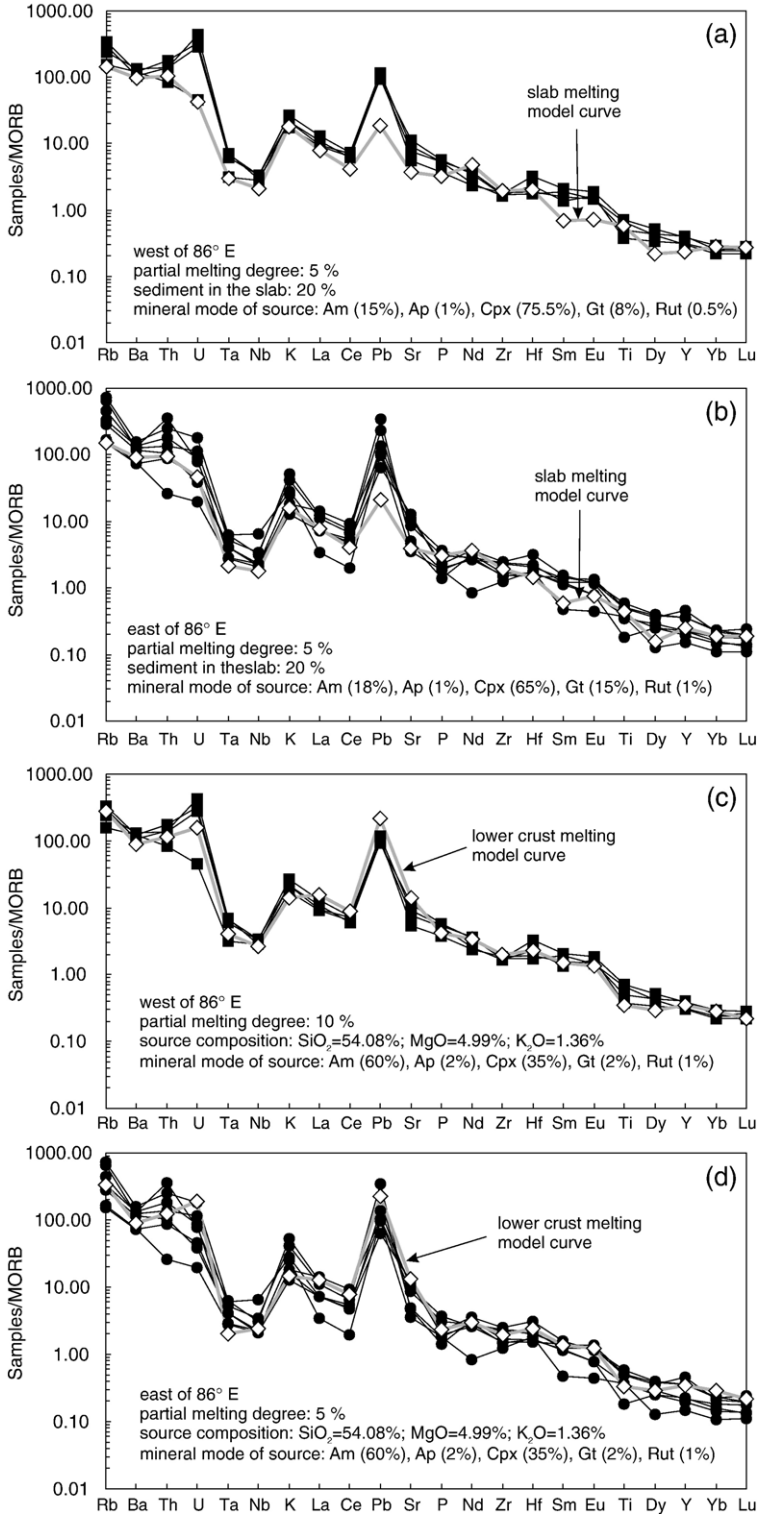

Fig. 9. Comparison between the observed data for the adakites and our model curves. (a) and (c) Adakites to the west of 86° E (longitude). (b) and (d) Adakites to the east of 86° E (longitude). The curve with open rhombs represents the results simulated by a non-modal batch melting model of the subducted slab (a, b) and lower crust (c, d). Am: amphibole; Ap: apatite; Cpx: clinopyroxene; Gt: garnet; Rut: rutile. Symbols are as in Fig. 2.

The lower Ba, Th, U and K contents predicted by the non-modal batch model compared to those of the adakites to the west of 86° E (Fig. 9c) could be explained by a small amount of mixing between K-rich mafic melts and the partial melts of the lower crust.

6.3.3. Subducted crust versus lower crustal melting models

On the basis of the above discussion it is clear that both partial melting of subducted oceanic crust with its cover of sediment and partial melting of mafic-intermediate meta-igneous rocks in the lower crust can produce credible fits to the trace element characteristics of the Lhasa terrane adakites and are consistent with their Sr–Nd–Pb isotope characteristics. So how do we chose between these competing models?

Arguments against partial melting of subducted oceanic crust could be made on thermal grounds (e.g., the subducted crust is likely to be too cold during the end stages of continent–continent collision). Additionally any silica-rich adakitic melt produced at mantle depths would be highly reactive towards the surrounding mantle peridotite as it rose towards the surface. If the adakitic magmas were produced by this process they would be unique amongst the spectrum of adakites worldwide (e.g. Hou et al., 2004) in requiring a significant proportion of subducted sediment in the source to account for their Sr–Nd–Pb isotope characteristics. Thus, an origin of the adakitic magmas by partial melting of subduction-modified lower crust seems the most attractive model. The heat required to melt hydrous (i.e. amphibole-bearing) meta-igneous rocks at a depth of 60–70 km could easily be supplied by the contemporaneous potassic–ultrapotassic magmas combined with crustal heating induced by lithospheric extension. Previous studies have suggested that the potassic and ultrapotassic magmas originated either by partial melting of the lithospheric mantle (e.g. Miller et al., 1999; Williams et al., 2001, 2004) or the asthenospheric mantle (Guo et al., 2006).

6.4. Constraints on the timing of uplift of the southern Tibetan Plateau provided by the post-collisional adakites

The similar age range of the post-collisional adakites (26.2–10.1 Ma) and the K-rich magmatic rocks (25.4–8.2 Ma) in the Lhasa terrane (Miller et al., 1999; Williams et al., 2001; Chung et al., 2003; Ding et al., 2003; Nomade et al., 2004; Williams et al., 2004) suggests that the post-collisional magmatism is associated with an important tectono-magmatic event which has influenced both the lower crust and the upper mantle. This could have involved the addition of water (or other fluids) to the lithosphere and/or asthenosphere, heating, or decompression (Niu, 2005). Northward underthrusting of the subducted Indian continental lithosphere beneath Tibet could have added water (or other fluids) to the wedge of asthenospheric mantle (e.g. Guo et al., 2006). A number of studies have attributed the generation of the post-collisional magmas (both adakites and K-rich magmatic rocks) in the Lhasa terrane to decomprssion melting induced by thinning of the sub-continental lithospheric mantle (e.g. Miller et al., 1999; Williams et al., 2001; Chung et al., 2003; Qu et al., 2004; Williams et al., 2004) or to break-off of the subducted slab (e.g. Kohn and Parkinson, 2002; Hou et al., 2004). Maheo et al. (2002), however, have argued that the narrow, linear belt of post-collisional magmatic rocks (including adakites) in the Lhasa terrane cannot be easily explained by the delamination of thickened lithosphere. Nomade et al. (2004) also emphasized that a model of convective thinning of the sub-continental lithospheric mantle fails to explain the age distribution and regional variations in the southern Tibetan Cenozoic volcanic rocks. Additionally, new petrological and geophysical studies (e.g. Deng et al., 2004; Zhou and Murphy, 2005; Guo et al., 2006) suggest that there is little evidence to support substantial Tertiary thickening of the Tibetan lithosphere, which is required by models involving its subsequent convective thinning (or delamination). Additionally, there is little evidence for subducted slab break-off beneath south Tibet at ~26 Ma. If slab break-off did occur and the post-collisional magmatism in south Tibet did indeed result from such a process, then we need to ask why the post-collisional magmatism (including adakites) only occurred between 26 and 8 Ma (e.g. Miller et al., 1999; Williams et al., 2001, 2004; Chung et al., 2003; Ding et al., 2003; Nomade et al., 2004).

Our field observations, together with data from previous studies (e.g. Williams et al., 2001; Hou et al., 2004), indicate a close correlation between the occurrence of post-collisional magmatism (including adakites and K-rich magmatic rocks) and a series of N–S-trending rifts within the Lhasa terrane (Fig. 1). This correlation has been attributed to east–west extension (e.g. Williams et al., 2001). The onset of east–west extension has been attributed to the elevation of the southern Tibetan Plateau to a height unsustainable by plate tectonic forces (Houseman et al., 1981; Dewey, 1988; England and Houseman, 1989; Harrison et al., 1992), signaling the tectonic collapse of the plateau (Coleman and Hodges, 1995; Searle, 1995). In the context of such a model the post-collisional adakites

and K-rich magmatic rocks in the Lhasa terrane can be interpreted as a consequence of decompression melting of the lower crust and upper mantle, respectively.

There is considerable disagreement about the timing of the onset of uplift and subsequent extensional collapse in the Lhasa terrane. Previous studies have indicated that east–west extension occurred at 18 Ma (Yin and Harrison, 2000; Williams et al., 2001), 17 Ma (Searle et al., 1997), 14 Ma (Coleman and Hodges, 1995; Searle, 1995), 11 Ma (Hodges et al., 1992; Hurtado et al., 2001) and 8 Ma (Harrison et al., 1992; Pan and Kidd, 1992; Harrison et al., 1995), perhaps suggesting semi-continuous lithospheric stretching in south Tibet between 18 and 8 Ma. Adakites and potassic–ultrapotassic magmatism within the Lhasa terrane range in age from 26 to 8 Ma (e.g. Miller et al., 1999; Williams et al., 2001; Chung et al., 2003; Ding et al., 2003; Nomade et al., 2004; Williams et al., 2004), suggesting that east–west extension may have already commenced by 26 Ma if their petrogenesis is indeed linked to lithospheric extension. We propose, therefore, that the onset of tectonic collapse of the southern Tibetan Plateau may be as early as 26 Ma. No outcrops of post-collisional adakites younger than 10 Ma (Coulon et al., 1986) have been found in the Lhasa terrane (Fig. 1), whilst the youngest reported age of the post-collisional K-rich magmatic rocks is 8.2 Ma (Ding et al., 2003), suggesting cessation of east–west extension at ~8–10 Ma. This conclusion is supported by the work of Wang et al. (2006), which provides evidence for significant uplift of south Tibet since ca. 7 Ma, perhaps indicating renewed compression. Thus, we propose that the post-collisional Lhasa terrane adakites and contemporaneous potassic–ultrapotassic magmatism provide an effective indicator for the timing of extensional collapse of the southern Tibetan Plateau.

Initiation of India–Asia collision occurred at ~50 Ma in the vicinity of Mt. Everest (Zhu et al., 2005), although this is not tightly constrained futher to the east. Rowley and Currie (2006) have suggested that the central part of the Tibetan Plateau has been characterized by elevations in excess of 4000 m since ~39 Ma and that once elevated the plateau did not collapse significantly. Additionally they find no evidence for plateau wide uplift in the late Miocene (~8–10 Ma) predicted by models which require convective destabilization of a thickened lithospheric mantle root. These findings are not necessarily inconsistent with our proposed model for the timing of E–W extension in the Lhasa terrane, provided that the amount of tectonic collapse is no more than a few hundred metres.

6.5. Significance of adakitic magmatism for the evolution of the Tibetan lithosphere

Fig. 10 indicates a schematic cross section of the ~74 km thick crust beneath the Lhasa terrane during the formation of the adakites (26–10 Ma). Primitive, K-rich magmas derived by partial melting of a sub-crustal mantle source (lithosphere or asthenosphere) cross the Moho and may stall in the lower crust or migrate rapidly to the surface along extensional fractures (dykes). These hot, mantle-derived magmas, will locally heat the surrounding lower crust causing partial melting of low melting point components.

The lower crust is likely to have been heavily modified during the preceding phase of subduction-related magmatism (153–40 Ma) when the Lhasa terrane formed part of an active continental margin. Evidence for the existence of this continental margin arc is provided by the exposures of Linzizong volcanic rocks and the Gangdese batholith within the Lhasa terrane (Fig. 1). The most primitive, mafic subduction-related magmas would have underplated and intruded the existing lower crust of the Lhasa terrane, undergoing AFC processes (Fig. 10). The resultant thickened lower crust would be highly heterogeneous, volatile-rich, and in the granulite or garnet–amphibolite

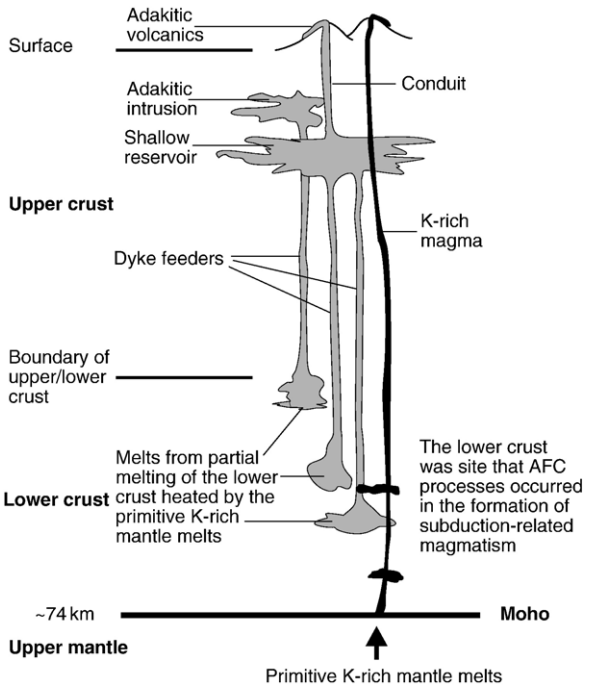

Fig. 10. Schematic crustal section during the formation of the post-collisional adakites in south Tibet (modified from Annen et al., 2006). The thickness of the crust beneath the Lhasa terrane (~74 km) is from Owens and Zandt (1997).

metamorphic facies. Mafic-intermediate subduction-related magmas crystallizing at pressures >20 kb within the lower crust would have feldspar-free mineral assemblages involving garnet+clinopyroxene+amphibole (±apatite and rutile), providing a suitable source for subsequent adakite magmatism. Interaction between the adakitic melts and ultramafic cumulates in the lower crust could most easily explain the compatible (i.e. Ni, Cr, V) trace element characteristics of the adakites.

7. Conclusions

Our geochemical data and modeling, combined with previous geochronological and geophysical data, support a model of partial melting of mafic-intermediate lower crust, rather than subducted slab melting or crustal AFC processes, as the best explanation of the petrogenesis of the post-collisional southern Tibetan (Lhasa terrane) adakites. The compositional differences between the adakites to the west and east of 86° E can be attributed to variable degrees of partial melting of the lower crust and to mixing with contemporaneous K-rich magmas which provide the heat source for crustal melting. The lower crustal source of the adakites was formed during an earlier phase of subduction-related magmatism in an active continental margin. The post-collisional adakites and potassic–ultrapotassic magmatism in the Lhasa terrane are attributed to extension-induced decompression melting caused by tectonic collapse of the southern Tibetan Plateau.

Acknowledgements

This study was financially supported by a joint project (2003–2005) between the Royal Society of London and the National Natural Science Foundation of China (NSFC). This work was also supported by the grants from the NSFC (40372045 and 40473023). We thank Z. Fan and Y.-L. Zhao for their help during the field work. Yaoling Niu is acknowledged for his enthusiastic help during this study. We thank Pat Castillo and an anonymous reviewer for their constructive comments, and Ruud Koole, journal manager, for help.

References

Aitchison, J.C., Badengzhu, Davis, A.M., Liu, J., Luo, H., Malpas, J.G., McDermid, I.R.C., Wu, H., Ziabrev, S.V., Zhou, M.-F., 2000. Remnants of a Cretaceous intra-oceanic subduction system within the Yarlung–Zangbo suture (southern Tibet). Earth Planet. Sci. Lett. 183, 231–244.

Annen, C., Sparks, R.S.J., 2002. Effects of repetitive emplacement of basaltic intrusions on thermal evolution and melt generation in the crust. Earth Planet. Sci. Lett. 203, 937–955.

Annen, C., Blundy, J.D., Sparks, R.S.J., 2006. The genesis of intermediate and silicic magmas in deep crustal hot zones. J. Petrol. 47, 505–539.

BGMRTAR (Bureau of Geology and Mineral Resources of Tibet Autonomous Region), 1993. Regional Geology of Tibet Autonomous Region. Geological Publishing House, Beijing, pp. 1–707 (in Chinese with English abstract).

Blisniuk, P.M., Hacker, B.R., Glodny, J., Ratschbacher, L., Bi, S., Wu, Z., McWilliams, M.O., Calvert, A., 2001. Normal faulting in central Tibet since at least 13.5 Myr ago. Nature 412, 628–632.

Bohrson, W.A., Spera, F.J., 2001. Energy-constrained open-system magmatic processes II: application of energy-constrained assimilation–fractional crystallization (EC-AFC) model to magmatic systems. J. Petrol. 42, 1019–1041.

Castillo, P.R., 2006. An overview of adakite petrogenesis. Chin. Sci. Bull. 51, 257–268.

Castillo, P.R., Janney, P.E., Solidum, R.U., 1999. Petrology and geochemistry of Camiguin Island, southern Philippines: insights to the source of adakites and other lavas in a complex arc setting. Contrib. Mineral. Petrol. 134, 33–51.

Chung, S.-L., Liu, D., Ji, J., Chu, M.-F., Lee, H.-Y., Wen, D.-J., Lo, C.-H., Lee, T.-Y., Qian, Q., Zhang, Q., 2003. Adakites from continental collision zones: melting of thickened lower crust beneath southern Tibet. Geology 31, 1021–1024.

Coleman, M., Hodges, K., 1995. Evidence for Tibetan Plateau uplift before 14 Myr ago from a new minimum age for east–west extension. Nature 374, 49–52.

Coulon, C., Maluski, H., Bollinger, C., Wang, S., 1986. Mesozoic and Cenozoic volcanic rocks from central and southern Tibet: $^{39}Ar/^{40}Ar$ dating, petrological characteristics and geodynamical significance. Earth Planet. Sci. Lett. 79, 281–302.

Defant, M.J., Drummond, M.S., 1990. Derivation of some modern arc magmas by melting of young subducted lithosphere. Nature 347, 662–665.

Defant, M.J., Drummond, M.S., 1993. Mount St. Helens: potential example of the partial melting of the subducted lithosphere in a volcanic arc. Geology 21, 547–550.

Defant, M.J., Richerson, P.M., de Boer, J.Z., Stewart, R.H., Maury, R.C., Bellon, H., Drummond, M.S., Feigenson, M.D., Jackson, T.E., 1991. Dacite genesis via both slab melting and differentiation: petrogenesis of La Yeguada volcanic complex, Panama. J. Petrol. 1101–1142.

Deng, J.F., Mo, X.X., Zhao, H.L., Wu, Z.X., Luo, Z.H., Su, S.G., 2004. A new model for the dynamic evolution of Chinese lithosphere: 'continental roots–plume tectonics'. Earth-Sci. Rev. 65, 223–275.

DePaolo, D.J., 1988. Neodymium Isotope Geochemistry: An Introduction. Springer Verlag, New York. 230 pp.

Dewey, J.F., 1988. Extensional collapse of orogens. Tectonics 7, 1123–1139.

Ding, L., Kapp, P., Zhong, D., Deng, W., 2003. Cenozoic volcanism in Tibet: evidence for a transition from oceanic to continental subduction. J. Petrol. 44, 1833–1865.

Elburg, M.A., van Bergen, M., Hoogewerff, J., Foden, J., Vroon, P., Zulkarnain, I., Nasution, A., 2002. Geochemical trends across an arc-continent collision zone: magma sources and slab-wedge transfer processes below the Pantar Strait volcanoes, Indonesia. Geochim. Cosmochim. Acta 66, 2771–2789.

England, P.C., Houseman, G., 1989. Extension during continental convergence, with application to the Tibetan Plateau. J. Geophys. Res. 94, 17561–17579.

Foley, S.F., Jackson, S.E., Fryer, B.J., Greenough, J.D., Jenner, G.A., 1996. Trace element partition coefficients for clinopyroxene and phlogopite in an alkaline lamprophyre from Newfoundland by LAM-ICP-MS. Geochim. Cosmochim. Acta 60, 629–638.

Garrison, J.M., Davidson, J.P., 2003. Dubious case for slab melting in the Northern volcanic zone of the Andes. Geology 31, 565–568.

Garrido, C.J., Bodinier, J.-L., Burg, J.-P., Zeilinger, G., Hussain, S.S., Dawood, H., Chaudhry, M.N., Gervilla, F., 2006. Petrogenesis of mafic garnet granulite in the lower crust of the Kohistan paleo-arc complex (Northern Pakistan): implications for intra-crustal differentiation of island arcs and generation of continental crust. J. Petrol. 47, 1873–1914.

GERM website: http://www.earthref.org/.

Goldstein, S.L., O'Nions, R.K., Hamilton, P.J., 1984. A Sm–Nd isotopic study of atmospheric dusts and particulates from major river systems. Earth Planet. Sci. Lett. 70, 221–236.

Green, T.H., 1994. Experimental studies of trace-element partitioning applicable to igneous petrogenesis—Sedona 16 years later. Chem. Geol. 117, 1–36.

Guo, Z., Hertogen, J., Liu, J., Pasteels, P., Boven, A., Punzalan, L., He, H., Luo, X., Zhang, W., 2005. Potassic magmatism in western Sichun and Yunnan provinces, SE Tibet, China: petrological and geochemical constraints on petrogenesis. J. Petrol. 46, 33–78.

Guo, Z., Wilson, M., Liu, J., Mao, Q., 2006. Post-collisional, potassic and ultrapotassic magmatism of the northern Tibetan Plateau: constraints on characteristics of the mantle source, geodynamic setting and uplift mechanisms. J. Petrol. 47, 1177–1220.

Harrison, T.M., Copeland, P., Kidd, W.S.F., Yin, A., 1992. Raising Tibet. Science 255, 1663–1670.

Harrison, T.M., McKeegan, K.D., LeFort, P., 1995. Detection of inherited monazite in the Manaslu leucogranite by $^{208}Pb/^{232}Th$ ion microprobe dating: crystallization age and tectonic implications. Earth Planet. Sci. Lett. 133, 271–282.

Hart, S.R., 1984. A large-scale isotope anomaly in the Southern Hemisphere mantle. Nature 309, 753–757.

Hawkesworth, C.J., Turner, S.P., McDermott, F., Peate, D.W., van Calsteren, P., 1997a. U–Th isotopes in arc magmas: implications for element transfer from the subducted crust. Science 276, 551–555.

Hawkesworth, C., Turner, S., Peate, D., McDermott, F., van Calsteren, P., 1997b. Elemental U and Th variations in island arc rocks: implications for U-series isotopes. Chem. Geol. 139, 207–221.

Hodges, K.V., Parrish, R.R., Housh, T.B., Lux, D.R., Burchfiel, B.C., Royden, L.H., Chen, Z., 1992. Simultaneous Miocene extension and shortening in the Himalayan orogen. Science 258, 1466–1470.

Hofmann, A.W., 1997. Mantle geochemistry: the message from oceanic volcanism. Nature 385, 219–229.

Hou, Z.-Q., Gao, Y.-F., Qu, X.-M., Rui, Z.-Y., Mo, X.-X., 2004. Origin of adakitic intrusives generated during mid-Miocene east–west extension in southern Tibet. Earth Planet. Sci. Lett. 220, 139–155.

Houseman, G.A., McKenzie, D.P., Molnar, P., 1981. Convective instability of a thickened boundary layer and its relevance for the thermal evolution of continental convergent belts. J. Geophys. Res. 86, 6115–6132.

Huang, G.-C., Li, Z.-C., Qiu, R.-Z., Cai, Z.-Y., 2004. Gological and geochemical characteristics of volcanic rocks in Shiduo, western Gangdese, Tibet. Geoscience 18, 511–517 (in Chinese with English abstract).

Hurtado Jr., J.M., Hodges, K.V., Whipple, K., 2001. Neotectonics of the Thakkhola Graben and implications for Recent activity on the South Tibetan fault system in the central Nepal Himalaya. Geol. Soc. Amer. Bull. 113, 222–240.

Jacobsen, S.B., Wasserburg, G.J., 1980. Sm–Nd isotopic evolution of chondrites. Earth Planet. Sci. Lett. 50, 139–155.

Jiang, W., Mo, X., Zhao, C., Guo, T., Zhang, S., 1999. Geochemistry of granitoid and its mafic microgranular enclave in Gangdese belt, Qinghai–Xizang Plateau. Acta. Pet. Sin. 15, 89–97 (in Chinese with English abstract).

Jin, X., Zhu, H., 2000. Determination of 43 trace elements in rock samples by double focusing high resolution Inductively Coupled Plasma-Mass Spectrometry. Chin. J. Anal. Chem. 28, 563–567 (in Chinese with English abstract).

Kapp, P., Murphy, M.A., Yin, A., Harrison, T.M., Ding, L., Guo, J., 2003. Mesozoic and Cenozoic tectonic evolution of the Shiquanhe area of western Tibet. Tectonics 22. doi:10.1029/2001TC001332.

Kay, R.W., 1978. Aleutian magnesian andesites: melts from subducted Pacific Ocean crust. J. Volcanol. Geotherm. Res. 4, 117–132.

Kay, S.M., Ramos, V.A., Marquez, M., 1993. Evidence in Cerro Pampa volcanic rocks for slab-melting prior to ridge-trench collision in southern South America. J. Geol. 101, 703–714.

Kohn, M.J., Parkinson, C.D., 2002. Petrologic case for Eocene slab breakoff during the Indo-Asian collision. Geology 30, 591–594.

Le Bas, M.J., Le Maitre, R.W., Streckeisen, A., Zanettin, B.A., 1986. Chemical classification of volcanic rocks based on the total alkali-silica diagram. J. Petrol. 27, 745–750.

Le Maitre, R.W., Bateman, P., Dudek, A., Keller, J., Lameyre, J., Le Bas, M.J., Sabine, P.A., Schmid, R., Sorensen, H., Streckeisen, A., Woolley, A.R., Zanettin, B., 1989. A Classification of Igneous Rocks and A Glossary of Terms. Blackwell, Oxford, England.

Lugmair, G.W., Marti, K., 1978. Lunar initial $^{143}Nd/^{144}Nd$: differential evolution of the lunar crust and mantle. Earth Planet. Sci. Lett. 39, 349–357.

Maheo, G., Guillot, S., Blichert-Toft, J., Rolland, Y., Pecher, A., 2002. A slab breakoff model for the Neogene thermal evolution of South Karakorum and South Tibet. Earth Planet. Sci. Lett. 195, 45–58.

Mahoney, J.J., Natland, J.H., White, W.M., Poreda, R., Bloomer, S.H., Fisher, R.L., Baxter, A.N., 1989. Isotopic and geochemical provinces of the western Indian Ocean spreading centers. J. Geophys. Res. 94, 4033–4052.

Martin, H., 1999. Adakitic magmas: modern analogues of Archaean granitoids. Lithos 46, 411–429.

McCulloch, M.T., Black, L.P., 1984. Sm–Nd isotopic systematics of Enderby Land granulites and evidence for the redistribution of Sm and Nd during metamorphism. Earth Planet. Sci. Lett. 71, 46–58.

Miller, C., Schuster, R., Kloetzli, U.S., Frank, W., Purtscheller, F., 1999. Post-collisional potassic and ultrapotassic magmatism in SW Tibet: geochemical and Sr–Nd–Pb–O isotopic constraints for mantle source characteristics and petrogenesis. J. Petrol. 40, 1399–1424.

Mo, X.X., Zhao, Z.D., Deng, J.F., Dong, G.C., Zhou, S., Guo, T.Y., Zhang, S.Q., Wang, L.L., 2003. Response of volcanism to the India–Asia collision. Earth Sci. Front. 10, 135–148 (in Chinese with English abstract).

Murphy, M.A., Yin, A., Harrison, T.M., Durr, S.B., Chen, Z., Ryerson, F.J., Kidd, W.S.F., Wang, X., Zhou, X., 1997. Did the Indo-Asian collision alone create the Tibetan Plateau? Geology 25, 719–722.

Niu, Y., 2005. Generation and evolution of basaltic magmas: some basic concepts and a new view on the origin of Mesozoic–Cenozoic basaltic volcanism in eastern China. Geol. J. China Univ. 11, 9–46.

Nomade, S., Renne, P.R., Mo, X., Zhao, Z., Zhou, S., 2004. Miocene volcanism in the Lhasa Block, Tibet: spatial trends and geodynamic implications. Earth Planet. Sci. Lett. 221, 227–243.

Owens, T.J., Zandt, G., 1997. Implications of crustal property variations for models of Tibetan Plateau evolution. Nature 387, 37–43.

Pan, G., Ding, J., 2004. An Explanation of Geological Map of the Tibetan Plateau and its neighboring Region (1:1500000). Chengdu Map Press, Chengdu. 133 pp (in Chinese).

Pan, Y., Kidd, W.S.F., 1992. Nyainqentanglha shear zone: a late Miocene extensional detachment in the southern Tibetan Plateau. Geology 20, 775–778.

Pan, G., Chen, Z., Li, X., Yan, Y., Xu, X., Xu, Q., Jiang, X., Wu, Y., Luo, J., Zhu, T., Peng, Y., 1997. Geological-Tectonic Evolution in the Eastern Tethys. Geological Publishing House, Beijing, pp. 1–191 (in Chinese with English abstract).

Pan, G., Wang, L., Zhu, D., 2004. Thoughts on some important scientific problems in regional geological survey of the Qinghai–Tibet Plateau. Geol. Bull. Chin. 23, 12–19 (in Chinese with English abstract).

Pearce, J.A., Mei, H., 1988. Volcanic rocks of the 1985 Tibet geotraverse: Lhasa to Golmud. Philos. Trans. R. Soc. Lond. A327, 169–201.

Pearce, J.A., Parkinson, I.J., 1993. Trace element models for mantle melting; application to volcanic arc petrogenesis. Geol. Soc. Spec. Publ. 76, 373–403.

Petford, N., Gallagher, K., 2001. Partial melting of mafic (amphibolitic) lower crust by periodic influx of basaltic magma. Earth Planet. Sci. Lett. 193, 483–499.

Plank, T., Langmuir, C.H., 1998. The chemical composition of subducting sediment and its consequences for the crust and mantle. Chem. Geol. 145, 325–394.

Qiu, R.-Z., Zhou, S., Deng, J.-F., Li, J.-F., Xiao, Q.-H., Cai, Z.-Y., 2004. Dating of gabbro in the Shemalagou ophiolite in the western segment of the Bangong Co-Nujiang ophiolite belt, Tibet—with a discussion of the age of the Bangong Co-Nujiang ophiolite belt. Geol. Chin. 31, 262–268 (in Chinese with English abstract).

Qu, X., Hou, Z., Li, Y., 2004. Melt components derived from a subducted slab in late orogenic ore-bearing porphyries in the Gangdese copper belt, southern Tibetan Plateau. Lithos 74, 131–148.

Rapp, R.P., Watson, E.B., 1995. Dehydration melting of metabasalt at 8–32 kbar: implications for continental growth and crust-mantle recycling. J. Petrol. 36, 891–931.

Rapp, R.P., Shimizu, N., Norman, M.D., Applegate, G.S., 1999. Reaction between slab-derived melts and peridotite in the mantle wedge: experimental constraints at 3.8 GPa. Chem. Geol. 160, 335–356.

Rehkämper, M., Hofmann, A.W., 1997. Recycled ocean crust and sediment in Indian ocean MORB. Earth Planet. Sci. Lett. 147, 93–106.

Rickwood, P.C., 1989. Boundary lines within petrologic diagrams which use oxides of major and minor elements. Lithos 22, 247–263.

Rowley, D.B., Currie, B.S., 2006. Paleo-altimetry of the late Eocene to Miocene Lunpola basin, central Tibet. Nature 439, 677–681.

Sajona, F.G., Maury, R.C., Pubellier, M., Leterrier, J., Bellon, H., Cotten, J., 2000. Magmatic source enrichment by slab-derived melts in a young post-collision setting, central Mindanao (Philippines). Lithos 54, 173–206.

Scharer, U., Xu, R.-H., Allegre, C.J., 1984. U–Pb geochronology of Gangdese (Transhimalaya) plutonism in the Lhasa–Xigaze region, Tibet. Earth Planet. Sci. Lett. 69, 311–320.

Searle, M., 1995. Plate tectonics: the rise and fall of Tibet. Nature 374, 17–18.

Searle, M.P., Parrish, R.R., Hodges, K.V., Hurford, A., Ayres, M.W., Whitehouse, M.J., 1997. Shisha Pangma leucogranite, South Tibetan Himalaya: field relations, geochemistry, age, origin, and emplacement. J. Geol. 105, 295–317.

Sen, C., Dunn, T., 1994. Dehydration melting of a basaltic composition amphibolite at 1.5 and 2.0 Gpa: implications for the origin of adakites. Contrib. Mineral. Petrol. 117, 394–409.

Song, Q., 1999. Geochemical features of the volcanic rocks of Linzizong group in Cuoqin Basin. J. Geomech. 5, 65–70 (in Chinese with English abstract).

Steiger, R.H., Jager, E., 1977. Subcommission on geochronology: convention on the use of decay constants in geo-and cosmochronology. Earth Planet. Sci. Lett. 36, 359–362.

Sun, S.-S., McDonough, W.F., 1989. Chemical and isotopic systematics of ocean basalts: implications for mantle composition and processes. In: Saunders, A.D., Norry, M.J. (Eds.), Magmatism in the Ocean Basins. Special Publications, vol. 42. Geological Society, London, pp. 313–345.

Tsuchiya, N., Kanisawa, S., 1994. Early Cretaceous Sr-rich silicic magmatism by slab melting in the Kitakami Mountains, Northeast Japan. J. Geophys. Res. 99, 22205–22220.

Turner, S., Hawkesworth, C., Liu, J., Rogers, N., Kelley, S., van Calsteren, P., 1993. Timing of Tibetan uplift constrained by analysis of volcanic rocks. Nature 364, 50–54.

Turner, S., Arnaud, N., Liu, J., Rogers, N., Hawkesworth, C., Harris, N., Kelley, S., van Calsteren, P., Deng, W., 1996. Post-collision, shoshonitic volcanism on the Tibetan Plateau: implications for convective thinning of the lithosphere and the source of ocean island basalts. J. Petrol. 37, 45–71.

Turner, S., Hawkesworth, C., Rogers, N., Bartlett, J., Worthington, T., Hergt, J., Pearce, J., Smith, I., 1997. ^{238}U–^{230}Th disequilibria, magma petrogenesis, and flux rates beneath the depleted Tonga-Kermadec island arc. Geochim. Cosmochim. Acta 61, 4855–4884.

Wang, Y., Deng, T., Biasatti, D., 2006. Ancient diets indicate significant uplift of southern Tibet after ca. 7 Ma. Geology 34, 309–312.

White, W.M., Hofmann, A.W., Puchelt, H., 1987. Isotope geochemistry of Pacific mid-ocean ridge basalt. J. Geophys. Res. 92, 4881–4893.

Williams, H., Turner, S., Kelley, S., Harris, N., 2001. Age and composition of dikes in Southern Tibet: new constraints on the timing of east–west extension and its relationship to postcollisional volcanism. Geology 29, 339–342.

Williams, H.M., Turner, S.P., Pearce, J.A., Kelley, S.P., Harris, N.B.W., 2004. Nature of the source regions for post-collisional, potassic magmatism in Southern and Northern Tibet from geochemical variations and inverse trace element modeling. J. Petrol. 45, 555–607.

Wilson, M., 1989. Igneous Petrogenesis: A Global Tectonic Approach. Unwin Hyman, London. 466 pp.

Wu, X.-L., Feng, Y., Huang, J.-P., 2005. Geochemical characteristics of Nianbo Formation at Cuoqin County, Tibet and its geotectonic significance. J. East China Inst. Technol. 28, 5–11 (in Chinese with English abstract).

Yin, A., Harrison, T.M., 2000. Geologic evolution of the Himalayan–Tibetan orogen. Ann. Rev. Earth Planet. Sci. 28, 211–280.

Yin, A., Harrison, T.M., Ryerson, F.J., Chen, W., Kidd, W.S.F., Copeland, P., 1994. Tertiary structural evolution of the Gangdese thrust system, southeastern Tibet. J. Geophys. Res. 99, 18175–18201.

Yogodzinski, G.M., Volynets, O.N., Koloskov, A.V., Seliverstov, N.I., Matvenkov, V.V., 1994. Magnesian andesites and the subduction component in a strongly calc-alkaline series at Piip Volcano, far western Aleutians. J. Petrol. 35, 163–204.

Yogodzinski, G.M., Kay, R.W., Volynets, O.N., Koloskov, A.V., Kay, S.M., 1995. Magnesian andesite in the western Aleutian Komandorsky region: implications for slab melting and processes in the mantle wedge. Geol. Soc. Amer. Bull. 107, 505–519.

Zhang, S.Q., 1996. Mesozoic and Cenozoic volcanism in central Gangdese: implications for lithospheric evolution of the Tibetan Plateau. Ph. D. thesis in Beijing: China University of Geosciences (in Chinese with English abstract).

Zhang, J., Ding, L., 2003. East–west extension in Tibetan Plateau and its significance to tectonic evolution. Chin. J. Geol. 38, 179–189 (in Chinese with English abstract).

Zhao, Z.D., Mo, X.X., Zhang, S.Q., Guo, T.Y., Zhou, S., Dong, G.C., Wang, Y., 2001. Post-collisional magmatism in Wuyu basin, central Tibet: evidence for recycling of subducted Tethyan oceanic crust. Sci. China (D) 44, 27–34.

Zhou, H.-W., Murphy, M.A., 2005. Tomographic evidence for wholesale underthrusting of India beneath the entire Tibetan Plateau. J. Asian Earth Sci. 25, 445–457.

Zhu, B., Kidd, W.S.F., Rowley, D.B., Currie, B.S., Shafique, N., 2005. Age of Initiation of the India–Asia collision in the East-Central Himalaya. J. Geol. 113, 265–285.